Shape Analysis of Planar Multiply-Connected Objects Using Conformal Welding

Lok Ming Lui, Wei Zeng, Shing-Tung Yau, and Xianfeng Gu, *Member, IEEE*

Abstract—Shape analysis is a central problem in the field of computer vision. In 2D shape analysis, classification and recognition of objects from their observed silhouettes are extremely crucial but difficult. It usually involves an efficient representation of 2D shape space with a metric, so that its mathematical structure can be used for further analysis. Although the study of 2D simply-connected shapes has been subject to a corpus of literatures, the analysis of *multiply-connected* shapes is comparatively less studied. In this work, we propose a representation for general 2D multiply-connected domains with arbitrary topologies using *conformal welding*. A metric can be defined on the proposed representation space, which gives a metric to measure dissimilarities between objects. The main idea is to map the exterior and interior of the domain conformally to unit disks and circle domains (unit disk with several inner disks removed), using holomorphic 1-forms. A set of diffeomorphisms of the unit circle $\mathbb{S}^1$ can be obtained, which together with the conformal modules are used to define the shape signature. A shape distance between shape signatures can be defined to measure dissimilarities between shapes. We prove theoretically that the proposed shape signature uniquely determines the multiply-connected objects under suitable normalization. We also introduce a reconstruction algorithm to obtain shapes from their signatures. This completes our framework and allows us to move back and forth between shapes and signatures. With that, a morphing algorithm between shapes can be developed through the interpolation of the Beltrami coefficients associated with the signatures. Experiments have been carried out on shapes extracted from real images. Results demonstrate the efficacy of our proposed algorithm as a stable shape representation scheme.

Index Terms—Shape analysis, shape signature, multiply-connected shapes, conformal welding, conformal modules, morphing

1 Introduction

The study of geometric shapes from their observed silhouettes is a crucial problem in the field of vision with many different applications, such as classification, recognition and image retrieval. In order to study shapes effectively, a common approach is to look for an efficient representation for the collection of all shapes, and define a robust metric on the representation space to measure their dissimilarities.

Finding a simple shape representation is however difficult, due to the complicated structure of the space of all shapes. For example, the set of shapes has no linear structure and is inherently infinite dimensional [15]. Designing a suitable representation for the space of all shapes becomes a big challenge. Recently, many different representations for 2D shapes and various measures of dissimilarity between them have been proposed [1]–[10], [15]–[20]. For example, Zhu *et al*. [1] proposed the representation of shapes using their medial axis and compare their skeletal graphs through a branch and bound strategy. Liu *et al*. [2] used shape axis trees to represent shapes, which are defined by the locus of midpoints of optimally corresponding boundary points. Belongie *et al*. [3] proposed to represent and match 2D shapes for object recognition, based on the shape context and the Hungarian method. Mokhtarian [4] introduced a multi-scale, curvature-based shape representation technique for planar curves, which is especially suitable for recognition of a noisy curve. Besides, various statistical models for shape representation were also proposed by different research groups [5]–[7]. These approaches provide a simple way to represent shapes with finite dimensional spaces, although they cannot capture all the variability of shapes. Yang *et al*. [8] proposed a signal representation called the Schwarz representation and applied it to shape matching problems. Lee *et al*. [9] proposed to represent curves using harmonic embedding through their complete silhouettes. Lipman *et al*. [10] proposed to detect shape dissimilarities up to isometry using conformal densities. In the past few years, several shape space models involving Riemannian manifolds of shapes have been proposed [28]–[36]. For example, models of deformable templates have been proposed to represent shapes based on deformations represented by diffeomorphisms acting on landmarks, curves, surfaces or other structures [28]–[32]. Sharon and Mumford [15] proposed a conformal approach to model simple closed curves which captured subtle variability of shapes up to scaling and translation. They also introduced a metric, called the Weil-Petersson metric, on the proposed

- L. M. Lui is with the Department of Mathematics, Chinese University of Hong Kong, Hong Kong. E-mail: lmlui@math.cuhk.edu.hk.
- W. Zeng is with the School of Computing and Information Sciences, Florida International University, Miami, FL 33199 USA. E-mail: wzeng@cs.fiu.edu.
- S.-T. Yau is with the Department of Mathematics, Harvard University, Cambridge, MA 02138, USA. E-mail: yau@math.harvard.edu.
- X. Gu is with the Department of Computer Science, State University of New York at Stony Brook, Stony Brook, New York, NY 11794-4400 USA. E-mail: gu@cs.sunysb.edu.

Manuscript received 3 July 2012; revised 14 Mar. 2013; accepted 14 May 2013. Date of publication 3 Nov. 2013; date of current version 13 June 2014. Recommended for acceptance by N. Paragios.
For information on obtaining reprints of this article, please send e-mail to: reprints@ieee.org, and reference the Digital Object Identifier below.
Digital Object Identifier 10.1109/TPAMI.2013.215

representation space. Conformal maps are also used for the shape analysis of Riemann surfaces embedded in $\mathbb{R}^3$. Zeng *et al*. [12], [13] analyzed 3D surfaces based on conformal modules. Their shape index can only determine shapes up to conformal deformations.

Most of the above methods work only on simple closed curves and generally cannot deal with multiply-connected objects. In real world applications, objects from their observed silhouettes are usually multiply-connected domains (i.e. domains with holes in the interior). In order to analyze such kind of shapes effectively, it is necessary to develop an algorithm which can deal with multiply-connected domains. Although the analysis of simply-connected shapes has been widely studied, the analysis of multiply-connected shapes is comparatively less studied. This motivates us to look for a good representation, which is equipped with a metric, to model planar objects of arbitrary topologies.

In this paper, we extend Sharon-Mumford conformal approach [15], which models 2D simply-connected domains, to represent multiply-connected shapes. Sharon-Mumford's approach provides an effective way to represent 2D simple curves and capture their subtle differences. To extend it to multiply-connected shapes, the key idea of our method is to map the exterior and interior of the domain conformally to unit disks and circle domains, using holomorphic 1-forms. A set of diffeomorphisms from the unit circle $\mathbb{S}^1$ to itself can be obtained, which together with the conformal modules are used to define the shape signature. Our proposed signature uniquely determines shapes with arbitrary topologies under suitable normalization. We also introduce a reconstruction algorithm to obtain shapes from their signatures. This completes our framework and allows us to move back and forth between shapes and signatures. With the reconstruction scheme, a morphing algorithm between shapes can also be developed through the interpolation of Beltrami coefficients associated with the shape signatures. Last but not least, the proposed representation space also inherits a metric, which can be used to measure dissimilarity between shapes. Preliminary results have been reported in [25].

In short, the contributions of this work are as follows: (i) we present a representation for the space of multiply-connected shapes using conformal modules and a set of diffeomorphisms(conformal weldings) of the unit circles. The representation uniquely determines the shape and can be considered as a unique 'fingerprint' for the shape; (ii) we present a reconstruction scheme to obtain shapes from their signatures, which allows us to go back and forth between shapes and signatures; (iii) we propose a simple metric on the representation space, which allows us to measure shape dissimilarities quantitatively and; (iv) we present a simple shape morphing algorithm between multiply-connected objects, by interpolating the Beltrami coefficients associated with the shape signatures.

The paper is organized as follows: Section 2 introduces the theoretic background, including the existence and the uniqueness of conformal/quasi-conformal mappings and the theory of conformal welding signature for simply connected domains; Section 3 proves the main theorem of the current work: the planar multiple connected shape and its signature are mutually determined by each other; Section 4 defines a Riemannian metric for the proposed signature space; Section 5 explains the implementation details thoroughly; Section 6 reports our experimental results. The paper is concluded in Section 7, where we point out future directions.

2 Theoretical Background

2.1 Quasiconformal Mappings and Beltrami Equation

Let $f:\Omega \subseteq \mathbb{C} \to \mathbb{C}$ be a complex function. The following differential operators are more convenient for the discussion

$$\frac{\partial}{\partial z}:=\frac{1}{2}\left(\frac{\partial}{\partial x}-i\frac{\partial}{\partial y}\right),\ \frac{\partial}{\partial \bar{z}}:=\frac{1}{2}\left(\frac{\partial}{\partial x}+i\frac{\partial}{\partial y}\right).$$

f is said to be *quasi-conformal* associated to μ if it is orientation-preserving and satisfies the following *Beltrami equation*:

$$\frac{\partial f}{\partial \bar{z}}=\mu(z)\frac{\partial f}{\partial z} \tag{1}$$

where $\mu(z)$ is some complex-valued Lebesgue measurable function satisfying $||\mu||_\infty:=\sup|\mu|<1$. In terms of the metric tensor, consider the effect of the pullback under f of the usual Euclidean metric ds_E^2; the resulting metric is given by:

$$f^*\left(ds_E^2\right)=\left|\frac{\partial f}{\partial z}\right|^2|dz+\mu(z)d\bar{z}|^2. \tag{2}$$

which, relative to the background Euclidean metric dz and $d\bar{z}$, has eigenvalues $(1+|\mu|)^2\left|\frac{\partial f}{\partial z}\right|^2$ and $(1-|\mu|)^2\left|\frac{\partial f}{\partial z}\right|^2$. μ is called the *Beltrami coefficient*, which is a measure of non-conformality. In particular, the map f is conformal around a small neighborhood of p when $\mu(p)=0$. Infinitesimally, around a point p, f may be expressed with respect to its local parameter as follows:

$$\begin{aligned} f(z) &= f(p)+f_z(p)z+f_{\bar{z}}(p)\bar{z} \\ &= f(p)+f_z(p)(z+\mu(p)\bar{z}). \end{aligned} \tag{3}$$

If $\mu(z)=0$ everywhere, then f is called *conformal* or *holomorphic*. A conformal map satisfies the following well-known Cauchy-Riemann equation:

$$\frac{\partial f}{\partial \bar{z}}=0.$$

Inside the local parameter domain, f may be considered as a map composed of a translation to $f(p)$ together with a stretch map $S(z)=z+\mu(p)\bar{z}$, which is postcomposed by a multiplication of $f_z(p)$, which is conformal. All the conformal distortion of $S(z)$ is caused by $\mu(p)$. $S(z)$ is the map that causes f to map a small circle to a small ellipse (see Fig. 1). From $\mu(p)$, we can determine the angles of the directions of maximal magnification and shrinkage and the amount of them as well. Specifically, the angle of maximal magnification is $\arg(\mu(p))/2$ with magnifying factor $1+|\mu(p)|$; the angle of maximal shrinkage is the orthogonal angle $(\arg(\mu(p))-\pi)/2$ with shrinking factor $1-|\mu(p)|$. The distortion or dilation is given by:

$$K=(1+|\mu(p)|)/(1-|\mu(p)|). \tag{4}$$

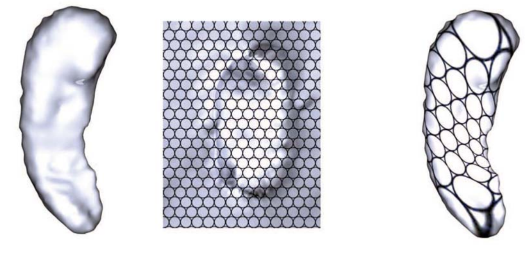

(a) (b) (c)

Fig. 1. (a) Shows the original hippocampus. (b) Shows the parameter domain with circle packing pattern. Under the quasiconformal parameterization, the infinitesimal circles on the parameter domain are mapped to infinitesimal ellipses on the hippocampus, as shown in (c).

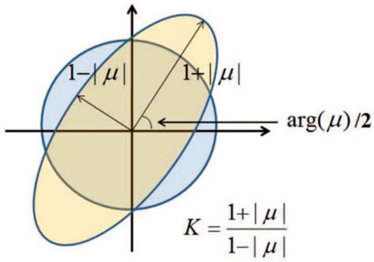

Fig. 2. Quasi-conformal maps infinitesimal circles to ellipses. The Beltrami coefficient measure the distortion or dilation of the ellipse under the QC map.

Thus, the Beltrami coefficient μ gives us important information about the properties of the map (See Fig. 2).

Given a compact simply-connected domain Ω in $\mathbb{C}$ and a Beltrami coefficient μ with $\|\mu\|_\infty < 1$. There is always a quasiconformal mapping from Ω to the unit disk $\mathbb{D}$ which satisfies the Beltrami equation in the distribution sense [21]. More precisely,

Theorem 2.1 (Measurable Riemann Mapping Theorem, see [22]). *Suppose Ω is a simply connected domain in $\mathbb{C}$ that is not equal to $\mathbb{C}$, and suppose that $\mu:\Omega \to \mathbb{C}$ is Lebesgue measurable and satisfies $\|\mu\|_\infty < 1$, then there is a quasiconformal homeomorphism ϕ from Ω to the unit disk, which is in the Sobolev space $W^{1,2}(\Omega)$ and satisfies the Beltrami equation (1) in the distribution sense.*

This theorem plays a fundamental role in the current work. Suppose $f, g:\mathbb{C} \to \mathbb{C}$ are with Beltrami coefficients μ_f, μ_g respectively. Then the Beltrami ceofficient for the composition $g \circ f$ is given by

$$\mu_{g \circ f} = \frac{\mu_f + (\mu_g \circ f)\tau}{1 + \bar{\mu}_f (\mu_g \circ f)\tau} \tag{5}$$

where $\tau = \frac{\bar{f}_z}{f_z}$.

2.2 Conformal Modules and Conformal Welding

Suppose Ω_1 and Ω_2 are planar domains. We say Ω_1 and Ω_2 are *conformally equivalent* if there is a biholomorphic diffeomorphism between them. All planar domains can be classified by the conformal equivalence relation. Each conformal equivalence class shares the same *conformal invariants*, the so-called *conformal module*. The conformal module is one of the key components for us to define the unique shape signature.

Suppose Ω is a compact domain on the complex plane $\mathbb{C}$. If Ω has a single boundary component, then it is called a *simply-connected domain*. Every simply-connected domain can be mapped to the unit disk conformally and all such kind of mappings differ by a *Möbius transformation*:

$$z \to e^{i\theta} \frac{z - z_0}{1 - \bar{z}_0 z}. \tag{6}$$

Denote the conformal parameterization of Ω onto the unit disk by $\Phi_1:\Omega \to \mathbb{D}$. Similarly, $\overline{\mathbb{C}}\backslash\Omega$ can be parameterized onto the unit disk by $\Phi_2:\overline{\mathbb{C}}\backslash\Omega \to \mathbb{D}$. The composition map

$$f: = \Phi_2 \circ \Phi_1^{-1}:\mathbb{S}^1 \to \mathbb{S}^1 \tag{7}$$

from the unit circle to itself is called the *conformal welding* of $\partial\Omega$. There is a close relationship between the domain Ω and the conformal welding f, which can be described as follows.

Definition 2.1 (Quasi-symmetric mapping). *A homeomorphism $f:\mathbb{R} \to \mathbb{R}$ is* quasi-symmetric *if there exists $M > 0$ such that*

$$\frac{1}{M} \le \frac{f(x+t) - f(x)}{f(x) - f(x-t)} \le M \tag{8}$$

for all $x \in \mathbb{R}$ and $t > 0$, and if $f(\infty) = \infty$. A homeomorphism $f:\mathbb{S}^1 \to \mathbb{S}^1$ is quasi-symmetric if $\phi \circ f \circ \phi^{-1}:\mathbb{R} \to \mathbb{R}$ is quasi-symmetric, where $\phi(z) = i\frac{1+z}{1-z}$.

In particular, if Ω is a Jordan domain, then the conformal welding of $\partial\Omega$ is quasi-symmetric [22]. Conversely, we have the following theorem.

Theorem 2.2 (Conformal welding of a simply-connected domain, see [22]). *Let $f:\mathbb{S}^1 \to \mathbb{S}^1$ be a quasisymmetric mapping. Then there exists a Jordan domain Ω and conformal mappings $\phi:\Omega \to \mathbb{D}$ and $\psi:\overline{\mathbb{C}}\backslash\Omega \to \overline{\mathbb{C}}\backslash\mathbb{D}$, such that*

$$f = \phi \circ \psi^{-1}$$

The domain Ω is unique up to a Möbius transformation.

In other words, every simply-connected domain can be determined by a conformal welding (up to a Möbius transformation). Our goal in this paper is to extend this theorem to multiply-connected domains.

Now, suppose Ω is a connected domain with multiple boundary components:

$$\partial\Omega = \gamma_0 - \gamma_1 - \gamma_2 \cdots \gamma_n,$$

where γ_0 represents the exterior boundary component. Ω is called a *multiply-connected domain*. A *circle domain* is a unit disk with circular holes. Two circle domains are conformally equivalent, if and only if they differ by a Möbius transformation. It turns out every multiply-connected domain can be conformally mapped to a circle domain, as described in the following theorem (see Fig. 3).

Theorem 2.3 (Riemann mapping for multiply-connected domain, see [26]). *If Ω is a multiply-connected domain, then there exists a conformal mapping $\phi:\Omega \to D$, where D*

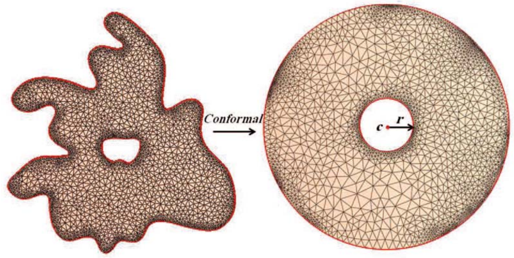

Fig. 3. Every multiply-connected domain can be mapped conformally to a circle domain (unit disk with inner disks removed). The conformal map is unique up to a Möbius transformation.

is a circle domain. Such kind of mappings differ by Möbius transformations.

Therefore, each multiply-connected domain is conformally equivalent to a circle domain. The conformal module for a circle domain is represented by the centers and radii of its inner boundary circles. All simply-connected domains are conformally equivalent. The topological annulus requires 1 parameter to represent the conformal module. Suppose now there are $n > 1$ inner circles. Since the Möbius transformation group is 3-dimensional, the conformal module requires $3n - 3$ parameters. We denote the conformal module of Ω_i by $Mod(\Omega_i)$.

Fix n, all conformal equivalence classes form a $3n - 3$ Riemannian manifold, called the *Teichmüller space*. The conformal module can be treated as the Teichmüller coordinates. The Weil-Peterson metric [15] is a Riemannian metric for Teichmüller space, which induces negative sectional curvature. Therefore, the geodesic between arbitrary two points is unique.

Suppose $\Gamma = \{\gamma_0, \gamma_1, \dots, \gamma_k\}$ are non-intersecting smooth closed curves on the complex plane. Γ segments the plane to a set of connected components:

$$\mathbb{C}^* = \Omega_0 \cup \Omega_1 \cup \cdots \cup \Omega_s,$$

with each segment Ω_i being a simply-connected or multiply-connected domain (See Fig. 5). We assume Ω_0 contains the infinity point and $p \notin \Omega_0$. By using a Möbius transformation

$$\phi(z) = \frac{1}{z - p},$$

p is mapped to ∞ and Ω_0 is mapped to a compact domain. We can replace Ω_0 by $\phi(\Omega_0)$. We then construct $\Phi_k{:}\Omega_k \to D_k$ to map each segment Ω_k to a circle domain D_k, $0 \le k \le s$.

Assume that $\gamma_k = \Omega_i \cap \Omega_j$, then $\Phi_i(\gamma_k)$ is a circular boundary on the circle domain D_i and $\Phi_j(\gamma_k)$ is another circular boundary on D_j. Let $f_{ij} = \Phi_i \circ \Phi_j^{-1}{:}\mathbb{S}^1 \to \mathbb{S}^1$ be the diffeomorphism from the unit circle to itself. f_{ij} is called the *conformal welding of* γ_k (please refer to Fig. 4 for the illustration). Here, we ignore the radii of $\Phi_i(\gamma_k)$ and $\Phi_j(\gamma_k)$, and treat both of them as $\mathbb{S}^1$.

The conformal modules and conformal weldings are the key components to define the unique signature of a multiply-connected shape.

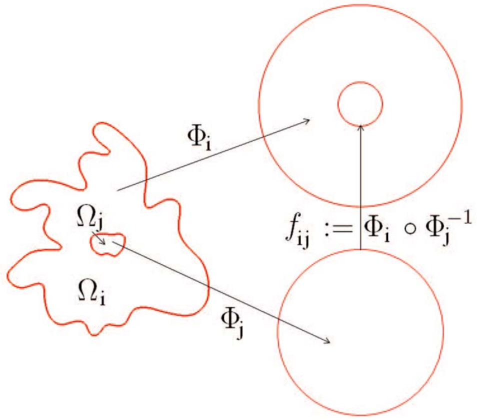

Fig. 4. Illustration of how conformal welding is defined as the composition map of the conformal parameterizations of the multiply-connected domain.

2.3 Circular Slit Map and Koebe's Iteration

In order to compute the conformal modules, one needs to map the multiply-connected domain to a circle domain. In the following, we introduce a general method, which can map a genus zero surface with multiple boundary components to a planar circle domain.

First, the multiply-connected domain (or surface) is conformally mapped to a planar annulus with concentric circular slits, based on Ahlfors' theorem:

Theorem 2.4 (Circular Slit Map, see [27]). *Suppose Ω is a multiply-connected domain with more than one boundary components, then there exists a conformal mapping $\phi{:}\Omega \to \mathbb{C}$, such that γ_0, γ_1 are mapped to concentric circles, other γ_k's are mapped to concentric circular slits. All such kind of mappings differ by a rotation.*

Fig. 6(b) shows the circular slit map for a triply-connected domain as shown in Fig. 6(a).

Second, the inner circular hole in the slit map image is filled as shown in Fig. 6(c) to form a disk with circular slits. Then the circular slit map is carried out on the disk with circular slits, as shown in Fig. 6(d). By repeating this procedure, all holes in the multiply-connected domain will be filled.

Finally, we perform Koebe's iteration. The disk that fills γ_1 is removed and the domain is conformally mapped to an annulus. The central hole is again filled again. Then we

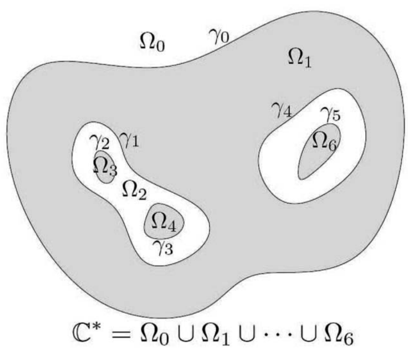

Fig. 5. Illustration of a family of non-intersecting closed contours which segment the complex plane into seven connected components.

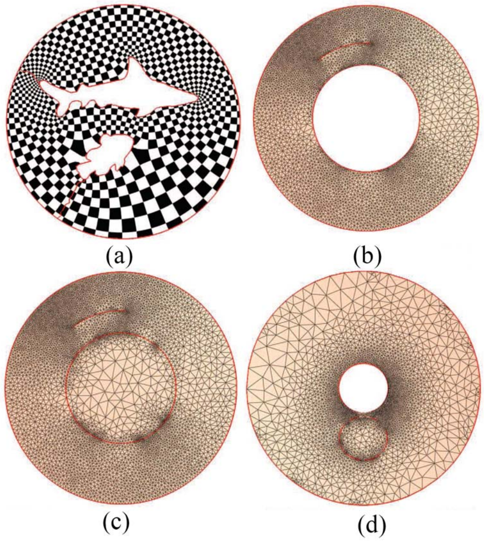

Fig. 6. Example of circular map. (a) Holomorphic l-form. (b) Circular slit map. (c) Fill the inner hole. (d) Circular map of (c).

repeat this for γ_2, then same procedure is performed on γ_3 and so on. By repeating this process, namely: deleting the disk inside γ_k; conformally mapped to an annulus; fill γ_k again. All holes will become rounder and rounder, and the image will converge to a circular domain under Möbius normalization. The proof of the convergence of the Koebe's iteration can be found in [26].

Theorem 2.5 (Koebe's iteration, see [26], page 502-505). *The Koebe's iteration converges to the conformal mapping from the multiple-connected domain to the circle domain under a Möbius normalization.*

3 Signatures by Conformal Welding

In this section, we describe how the shape signature of a multiply-connected shape is defined, which is based on its conformal modules and conformal weldings.

Given a shape Ω with $n+1$ non-intersecting boundaries $\Gamma = \{\gamma_0, \gamma_1, \ldots, \gamma_n\}$ on the complex plane. Suppose Γ segments the plane to a set of connected components $\{\Omega_0, \Omega_1, \ldots, \Omega_s\}$, where each component Ω_i is either a

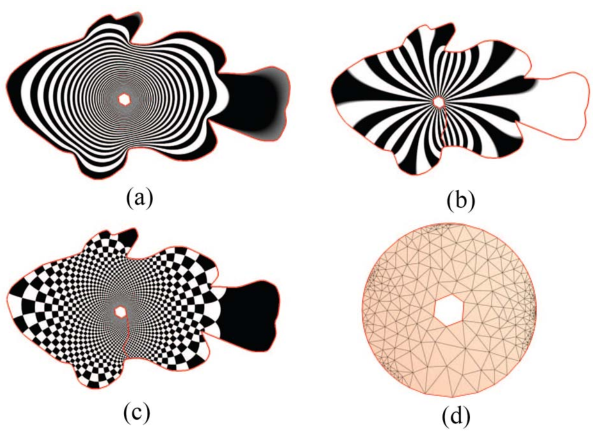

Fig. 7. Conformal mapping for a simply-connected domain by puncturing a small hole in the center. (a) Exact form. (b) Closed form. (c) Holomorphic l-form. (d) Conformal mapping.

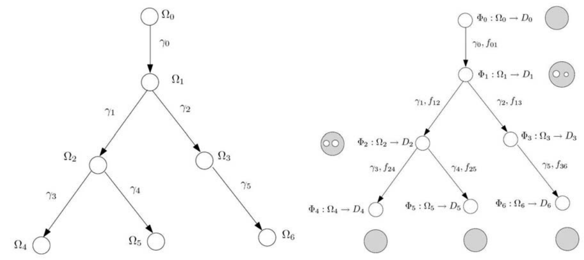

Fig. 8. Illustration of the proof of the Main Theorem (Theorem 3.1).

simply-connected or a multiply-connected domain. We can compute the conformal welding for each γ_k. This can be done by conformally parameterizing each component Ω_i onto the circle domain D_i, denote them by $\Phi_i:\Omega_i \to D_i$. Assume that $\gamma_k = \Omega_i \cap \Omega_j$. The conformal welding of γ_k is given by:

$$f_{ij}: = \Phi_i \circ \Phi_j^{-1}:\mathbb{S}^1 \to \mathbb{S}^1.$$

We also call the conformal welding f_{ij} of γ_k the *signature of* γ_k. Again, we ignore the radii of $\Phi_i(\gamma_k)$ and $\Phi_j(\gamma_k)$, and treat both of them as $\mathbb{S}^1$.

The signatures of all γ_k together with the conformal modules, $Mod(D_i)$, of all D_i define the shape signature of the multiply-connected shape Ω.

Definition 3.1 (Signature of a family of loops). *The signature of a family of non-intersecting planar closed curves* $\Gamma = \{\gamma_0, \gamma_1, \ldots, \gamma_n\}$ *is defined as*

$$S(\Gamma): = \{Mod(D_0), \ldots, Mod(D_s)\} \cup \{f_{ij}\}_{(i,j)\in I}.$$

where $I = \{(i,j):\Omega_i \cap \Omega_j \neq \phi\}$.

Note that if a circle domain D_k is a disk, its conformal module can be omitted from the signature.

The advantage of this proposed shape signature is that it determines a multiply-connected shape up to a Möbius transformation. This can be explained in more details by the following main theorem. This theorem plays a fundamental role for the current work.

Theorem 3.1 (Main Theorem). *The family of non-intersecting planar closed curves* Γ *is determined by its signature* $S(\Gamma)$, *uniquely up to a Möbius transformation of the Riemann sphere* $\mathbb{C} \cup \{\infty\}$. *The Möbius transformation of the Riemann sphere is given by* $(az+b)/(cz+d)$, *where* $ad - bc = 1, a, b, c, d \in \mathbb{C}$.

Proof. Suppose a family of planar smooth curves $\Gamma = \{\gamma_0, \ldots, \gamma_m\}$ divide the plane to segments $\{\Omega_0, \Omega_1, \cdots, \Omega_n\}$, where Ω_0 contains the ∞ point (See Fig. 5). We represent the segments and the curves as a tree as shown in Fig. 8(left), where each node represents a segment Ω_k, each link represents a curve γ_i. If Ω_j is included by Ω_i, and Ω_i and Ω_j shares a curve γ_k, then in the tree, the link γ_k connects Ω_j to Ω_i, denoted as $\gamma_k:\Omega_i \to \Omega_j$.

In Fig. 8(right), each segment Ω_k is mapped conformally to a circle domain D_k by $\Phi_k:D_k \to \Omega_k$. The signature for each closed curve γ_k is computed $f_{ij} = \Phi_i \circ \Phi_j^{-1}|_{\gamma_k}:[0,2\pi] \to [0,2\pi]$, where $\gamma_k:\Omega_i \to \Omega_j$ in the tree.

Let γ_k:$D_i \to D_j$, D_j be a leaf of the tree. For each point $z = re^{i\theta}$ in D_j, the *extension map*

$$G_{ij}(re^{i\theta}) = re^{\sqrt{-1}f_{ij}(\theta)}.$$

Suppose D_k is a circle domain, a path from the root D_0 to D_k is $\{i_0 = 0, i_1, i_2, \ldots, i_n = k\}$, then the map from G_k:$D_k \to S_k$: $= G_k(D_k)$ is given by

$$G_k = G_{i_0 i_1} \circ G_{i_1 i_2} \circ \cdots \circ G_{i_{n-1} i_n}.$$

Note that, by definition, G_0 is identity. Also, $S = S_0 \cup S_1 \cup \ldots \cup S_n$ is a Riemann sphere. Let F_k: $= \Phi_k \circ G_k^{-1}$:$S_k \to \Omega_k$. Define G_Γ:$S \to \Omega$ by:

$$G_\Gamma|_{S_k} = F_k$$

We first prove that G_Γ is a well-defined map from S to Ω. The values under the map G_Γ on γ_k can be defined either by $F_{i_{n-1}}$ or F_{i_n} (= F_k).We need to prove that $F_{i_{n-1}}|_{\gamma_k}$ = $F_{i_n}|_{\gamma_k}$. This is true since $F_{i_{n-1}}|_{\gamma_k} = \Phi_{i_{n-1}} \circ G_{i_{n-1}}^{-1}|_{\gamma_k}$ and $F_k|_{\gamma_k} = \Phi_{i_n} \circ G_{i_{n-1} i_n}^{-1} \circ G_{i_{n-1}}^{-1}|_{\gamma_k} = \Phi_{i_n} \circ \Phi_{i_n}^{-1} \circ \Phi_{i_{n-1}} \circ G_{i_{n-1}}^{-1}|_{\gamma_k} = \Phi_{i_{n-1}} \circ G_{i_{n-1}}^{-1}|_{\gamma_k}$.

Now the Beltrami coefficient μ of G_Γ can be easily computed. In particular, the Beltrami coefficient of G_k^{-1}:$S_k \to D_k$ can be directly computed, denoted it by μ_k:$S_k \to \mathbb{C}$. The composition F_k: $= \Phi_k \circ G_k^{-1}$:$S_k \to \Omega_k$ maps S_k to Ω_k. Since Φ_k is conformal, the Beltrami coefficient of $\Phi_k \circ G_k^{-1}$ is equal to μ_k. μ can be determined by $\mu|_{S_k} = \mu_k$.

The shape can then be determined from the shape signature by computing a map from the Riemann sphere S to the original Riemann sphere Ω, G_Γ:$S \to \Omega$ associated with the Beltrami-coefficient μ.

By theorem 2.1, the solution exists and unique up to a Möbius transformation. This proves the theorem. □

Due to the conformal ambiguity, the obtained conformal modules and conformal weldings of a multiply-connected shape are not unique. To remove the conformal ambiguity, a normalization must be performed. For the conformal parameterization of the outermost domain, we restrict it to fix the point ∞ (north pole). As for the the conformal parameterizations of the inner domains, we normalize them in such a way that each conformal weldings f_{ij} fixes the points -1,1 and i. After the normalization, the shape signature can determine the shape uniquely up to a translation, rotation and scaling. More precisely, it can be described as follows:

Theorem 3.2 (Normalization). *Suppose the shape signature is obtained by restricting the conformal parameterization of the outermost domain to fix ∞ (north pole). Assume that the conformal parameterizations of the inner domains are normalized. The shape signature $S(\Gamma)$ determines the shape uniquely up to a translation, rotation and scaling.*

Proof. According to the proof of the Main Theorem, every shape signature is associated with a Beltrami coefficient μ_Γ defined on the Riemann sphere S. The quasi-conformal map corresponding to μ_Γ can be reconstructed. The reconstructed quasi-conformal map is not unique. But it is unique up to a Möbius transformation. Let f_1:$S \to S$ and f_2:$S \to S$ be quasi-conformal maps corresponding to μ_Γ. Then $f_2^{-1} \circ f_1$ is a conformal map of the Riemann sphere. All conformal map of the Riemann sphere is given by

$$\phi(z) = \frac{az + b}{cz + d}$$

Suppose the conformal parameterization of the outermost domain is restricted to fix ∞ (north pole). Then $\phi(\infty) = \infty$ and hence the conformal map ϕ is of the form: $\phi(z) = az + b$. In other words, $f_1 = af_2 + b$. This implies the multiply-connected shapes reconstructed from f_1 and f_2 respectively differ by a translation, rotation and scaling. □

In fact, by restricting the conformal parameterization of the outermost domain to fix any three points, the obtained shape signature determines the shape uniquely.

Corollary 3.2 (Fixing three points). *By fixing any 3 points of the conformal parameterization of the outermost domain, the shape signature determines the shape uniquely.*

Proof. It follows from the proof of Theorem 3.2 that if the conformal parameterization of the outermost domain is restricted to fix any three points, the Möbius transformation $\phi(z)$ can be uniquely determined. In other words, the quasi-conformal map associated to μ_Γ is unique. Hence, the shape signature determines the shape uniquely. □

Sometimes, we might consider the multiply-connected shape to be embedded in a unit disk. By restricting the conformal parameterization of the outermost domain to fix the points -1, 1 and i, the shape signature can uniquely determine the shape. It can be explained by the following theorem:

Theorem 3.3 (Shape embedded in $\mathbb{D}$). *Let the multiply-connected shape be embedded in a unit disk $\mathbb{D}$. By restricting the conformal parameterization of the outermost domain to fix the points -1, 1 and i, the shape signature uniquely determines the shape.*

Proof. Similarly, the shape signature is associated with a Beltrami coefficient μ_Γ defined on the unit disk $\mathbb{D}$. The reconstructed quasi-conformal maps corresponding to $\mathbb{D}$ differ by a Möbius transformation of $\mathbb{D}$, which is given by

$$\phi(z) = e^{i\theta}\frac{z - a}{1 - \bar{a}z} \quad \text{where } a \in \mathbb{D}.$$

By restricting the conformal parameterization of the outermost domain to fix the points -1, 1 and i, $\phi(z)$ can be uniquely determined. Hence, the shape signature determines the shape uniquely. □

Therefore, one key advantage of the proposed shape signature is that it determines the associated shape uniquely up to some transformations. Given a shape signature, one can reconstruct its associated shape. We explain in details how shapes can be reconstructed from their shape signatures.

The reconstruction scheme follows from the proof of the Main Theorem. Let $\Gamma = \{\{c_{ij}, r_{ij}\}_{j=i}^{n_i}\}_{i=1}^{n} \cup \{f_{ij}\}_{(i,j)\in I}$ be the shape signature of a multiply-connected shape $\Omega = \Omega_0 \cup \Omega_1 \cup \ldots \cup \Omega_n$. Here, $I = \{(i,j)$:$\Omega_i \cap \Omega_j \neq \phi\}$. Suppose D_k is a circle domain and a path from D_0 to D_k is given by:

$$\{i_0 = 0, i_1, i_2, \ldots, i_n = k\}$$

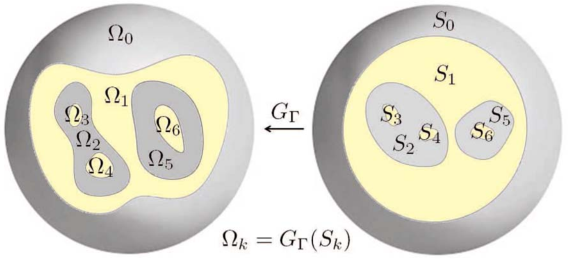

Fig. 9. Illustration of how G_Γ can be used to reconstruct the associated shape.

Here, a path is a sequence such that $\Omega_{i_{k-1}}$ and Ω_{i_k} shares a common boundary.

Compute the Beltrami coefficient μ_k of G_k^{-1} given by:

$$G_k = G_{i_0 i_1} \circ G_{i_1 i_2} \circ \dots \circ G_{i_{n-1} i_n}$$

where

$$G_{ij}\left(re^{i\theta}\right) = re^{\sqrt{-1}f_{ij}(\theta)}.$$

Let $S_k = G_k(D_k)$. The Riemann sphere S^2 can be expressed as the union of S_k's, namely, $S^2 = \bigcup_{k=0}^n S_k$. We can then compute the quasi-conformal map $G_\Gamma: S^2 \to S^2$ whose Beltrami coefficient is given by:

$$\mu_{G_\Gamma} = \mu_k \quad \text{on } S_k.$$

The multiply-connected shape $\Omega = \Omega_0 \cup \Omega_1 \cup \dots \cup \Omega_n$ can be reconstructed by:

$$\Omega_k = G_\Gamma(S_k) \quad \text{for } k = 0, 1, 2, \dots, n$$

(See Fig. 9 for an illustration).

Similarly, the multiply-connected shape embedded in the unit disk $\mathbb{D}$ can be reconstructed from its shape signature as well.

4 Metric on the Signature Space

To compare two shapes S_1 and S_2, it is important to have a metric measuring their geometric differences. The space of all shape signatures proposed in this paper inherits a metric, which can be used to measure shape differences. In this section, we describe how the metric can be constructed.

Let Υ_1 and Υ_2 be two shape signatures. Note that we assume the shape signatures are normalized to remove the conformal ambiguity. This can be done by normalizing the conformal parameterizations of the outer domain and inner domains, as discussed in Section 3.

To obtain a distance between two shape signatures, the correspondence of contours between two shapes must be assigned. The correspondence of contours can be adjusted by performing a permutation of contours at each level.

Suppose the shape signature Υ_k $(k = 0, 1)$ is given by:

$$\Upsilon_k = \{\mathbf{Mod}(D_i^k)\}_{i=1}^n \cup \{f_{ij}^k\}_{(i,j)\in I}$$

where

$$\mathbf{Mod}(D_i) = \{c_{ij}^k, r_{ij}^k\}_{j=1}^{n_i}$$

For $i = 1, 2, \dots n$, let σ_i be the permutation of $\{1, 2, \dots, n_i\}$, which is a permutation of the inner contours of D_i. A permutation of the shape signature is defined as:

$$(\sigma_1, \dots, \sigma_n)(\Upsilon_k) = \{\mathbf{Mod}(\sigma_i(D_i^k))\}_{i=1}^n \cup \{f_{i\sigma_i(j)}^k\}_{(i,j)\in I}$$

where

$$\mathbf{Mod}(\sigma_i(D_i^k)) := \{c_{i\sigma_i(j)}^k, r_{i\sigma_i(j)}^k\}_{j=1}^{n_i}$$

We can then define a distance between Υ_1 and Υ_2 as follows:

$$\begin{aligned}\mathbf{d_{shape}}(\Upsilon_1, \Upsilon_2) &= \min_{\sigma_1,\dots,\sigma_n} \mathbf{dist}(\Gamma_1, (\sigma_1, \dots, \sigma_n)(\Gamma_2)) \\ &:= \min_{\sigma_1,\dots,\sigma_n} \left\{ \sum_{(i,j)\in I} (|c_{ij}^1 - c_{i\sigma_i(j)}^2|^2 + |r_{ij}^1 - r_{i\sigma_i(j)}^2|^2 \right. \\ &\qquad \left. + \int_0^{2\pi} |f_{ij}^1 - f_{i\sigma_i(j)}^2| d\theta) \right\} \end{aligned} \tag{9}$$

Remark 4.1. The distance function $\mathbf{d_{shape}}$ defined in Equation (9) is a metric.

By direct computation, it is easy to verify that the distance function satisfies the following:

- $\mathbf{d_{shape}}(\Upsilon_1, \Upsilon_2) = \mathbf{d_{shape}}(\Upsilon_2, \Upsilon_1)$;
- $\mathbf{d_{shape}}(\Upsilon_1, \Upsilon_2) = 0$ if and only if $\Upsilon_1 \sim \Upsilon_2$;
- $\mathbf{d_{shape}}(\Upsilon_1, \Upsilon_2) + \mathbf{d_{shape}}(\Upsilon_2, \Upsilon_3) \geq \mathbf{d_{shape}}(\Upsilon_1, \Upsilon_3)$.

Under different normalization, the metric measures the dissimilarity between two shapes up to different transformations. Assume that the shapes are embedded in the whole 2D plane. Suppose the shape signature is obtained by restricting the conformal parameterization of the outermost domain to fix ∞ (north pole). Then the shape distance $\mathbf{d_{shape}}$ is equal to 0 if and only if two shapes are equal up to a translation, rotation and scaling. By restricting the conformal parameterization of the outermost domain to fix any three points, $\mathbf{d_{shape}} = 0$ if and only if two shapes are exactly the same.

Similarly, suppose the shapes are embedded in the unit disk $\mathbb{D}$. By restricting the conformal parameterization of the outermost domain to fix the points -1, 1 and i, $\mathbf{d_{shape}} = 0$ if and only if the two shapes are exactly equal.

Following the idea proposed in Sharon-Mumford model [15], one can also choose the Weil-Peterson metric for the metric on the signature space. We choose the above proposed metric for easier and faster computation. Experimental results on shape clustering show that our proposed metric is an effective metric for classifying shapes (see Section 6).

5 Implementation Details

Here, we assume a planar multiply-connected domain Ω has n inner boundary components. Let the boundaries of the mesh be $\partial\Omega = \gamma_0 - \gamma_1 \cdots - \gamma_n$. Suppose Ω is represented by a triangular mesh. We use v_i to denote a vertex, $[v_i, v_j]$ to denote an edge and $[v_i, v_j, v_k]$ to denote a face. The angle structure of the mesh is defined as follows:

Definition 5.1 (Angle Structure). *The angle at vertex v_i in a triangle $[v_i, v_j, v_k]$ is denoted as θ_{jk}^i. The angle structure of the mesh is defined as the set*

$$A(\Omega) := \{\theta_{jk}^i, \theta_{ij}^k, \theta_{ki}^j | [v_i, v_j, v_k] \in \Omega\}.$$

All the following computations depend solely on the angle structure of the mesh.

5.1 Discrete Holomorphic 1-Forms

Conformal parameterization plays an important role for our shape signature. In this work, the computation of the conformal parameterizations of the planar object onto circle domains rely on the *discrete holomorphic 1-forms*. In this subsection, we will explain how the discrete holomorphic 1-form can be computed.

Discrete Differential Operators: Discrete 0-forms are discrete functions defined on vertices, whereas discrete 1-forms and 2-forms are functions defined on edges and faces respectively satisfying compatibility conditions under the change of orientation. More specifically, for discrete 1-forms, $f([v_i, v_j]) = -f([v_j, v_i])$ for any edge $[v_i, v_j]$. For discrete 2-forms, $f([v_i, v_j, v_k]) = -f([v_j, v_i, v_k])$ for any face $[v_i, v_j, v_k]$.

The gradient of a 0-form f, df, is a discrete 1-form, which is given by

$$df([v_i, v_j]) = f(v_j) - f(v_i).$$

The *curl* of a discrete 1-form ω is given by

$$\begin{aligned} curl\ \omega([v_i, v_j, v_k]) &= \omega(\partial[v_i, v_j, v_k]) \\ &= \omega([v_i, v_j]) + \omega([v_j, v_k]) + \omega([v_k, v_i]). \end{aligned}$$

The *div* of ω is given by

$$div\ \omega(v_i) = \sum_{[v_i,v_j]\in\Omega} w_{ij}\ \omega([v_i, v_j]),$$

where w_{ij} is the *edge weight*, defined as the follows:

$$w_{ij} := \begin{cases} \cot\theta_{ij}^k + \cot\theta_{ji}^l & [v_i, v_j] \notin \partial\Omega \\ \cot\theta_{ij}^k & [v_i, v_j] \in \partial\Omega \end{cases}$$

where θ_{ij}^k and θ_{ij}^l are the corner angles on the faces adjacent to the edge $[v_i, v_j]$ and against the edge [37].

The *discrete wedge operator* $\wedge$ is defined as follows. Given $[v_i, v_j, v_k] \in \Omega$, τ_1, τ_2 are discrete 1-forms, then

$$\tau_1 \wedge \tau_2([v_i, v_j, v_k]) = \frac{1}{2}\begin{vmatrix} \tau_1([v_i, v_j]) & \tau_2([v_i, v_j]) \\ \tau_1([v_j, v_k]) & \tau_2([v_j, v_k]) \end{vmatrix}.$$

Discrete Harmonic Functions: Let f be a discrete function. We say f is a *discrete harmonic function*, if it satisfies the following equation:

$$div\ df(v_i) = 0, \forall v_i \notin \partial\Omega.$$

One can easily obtain n harmonic functions, $f_k:\Omega \to \mathbb{R}, k > 0$, which satisfies the above equation with the following boundary condition

$$f_k(v_i) = 1, \forall v_i \in \gamma_k, f_k(v_j) = 0, \forall v_j \in \partial\Omega \setminus \gamma_k.$$

Let $\tau_k = df_k, 1 \le k \le n$. Then $\{\tau_1, \tau_2, \ldots, \tau_n\}$ forms a basis for all exact harmonic 1-forms on Ω.

Discrete Harmonic 1-forms: A basis of the discrete closed harmonic 1-form group on Ω can be obtained. We first compute the shortest cut η_k from γ_k to γ_0, $1 \le k \le n$. Then we slice Ω along η_k to get an $\tilde{\Omega}_k$, such that the shortest path η_k becomes η_k^+ and η_k^-. Next, we construct a function $h_k:\tilde{\Omega}_k \to \mathbb{R}$, such that

$$h_k(p) = 1, \forall p \in \eta_k^+; \quad h_k(p) = 0, \forall p \in \eta_k^-;$$

and $h_k(p)$ is random for all interior vertices on $\tilde{\Omega}_k$. Then dh_k is a *discrete exact 1-form* on $\tilde{\Omega}_k$. Because of the consistency along the boundaries, dh_k is also a closed 1-form (but not exact) on Ω. We compute a function g_k such that $dh_k + dg_k$ is a harmonic 1-form by solving the equation,

$$div(dh_k + dg_k)(v_i) = 0, \forall v_i \notin \partial\Omega.$$

Let $\tau_{n+k}: = dh_k + dg_k, 1 \le k \le n$, then $\{\tau_{n+1}, \tau_{n+2}, \ldots, \tau_{2n}\}$ form the basis for all closed (non-exact) harmonic 1-form group on Ω. As a result, $\{\tau_1, \ldots, \tau_{2n}\}$ forms a basis for the discrete closed harmonic 1-form group on Ω (See Fig. 10).

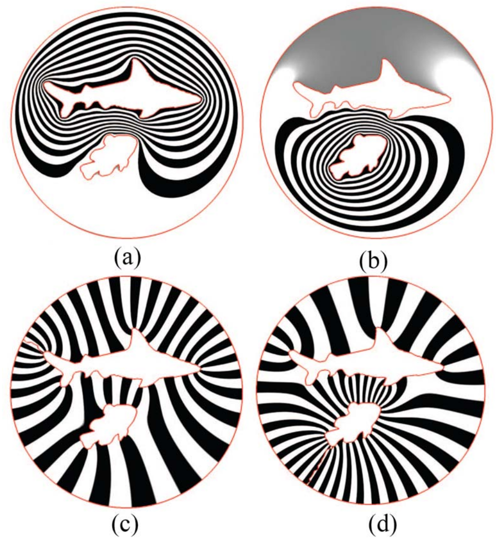

Fig. 10. Harmonic 1-form basis. (a) Exact form τ_1. (b) Exact 1-form τ_2. (c) Closed form τ_3. (d) Closed form τ_4.

Discrete Holomorphic Differential: A holomorphic 1-form can be constructed by a harmonic 1-form and its conjugate $\tau_k + i^*\tau_k$, where * is the Hodge star operator. The *discrete Hodge Star* * is defined as follows. Each face is an Euclidean triangle embedded in $\mathbb{R}^2$ with the isometric local coordinates (x, y). Suppose τ is a discrete closed 1-form, then it has a local representation $\omega = c_1dx + c_2dy$, where c_1, c_2 are constants on each face, $^*\omega = c_1dy - c_2dx$.

The conjugate form of a harmonic 1-form is still a harmonic 1-form. Therefore,

$$^*\tau_k = \sum_{i=1}^{2n} c_{ki}\tau_i,$$

where c_{ki}'s are unknown real numbers. In particular,

$$\int_\Omega \tau_j \wedge {}^*\tau_k = \sum_{i=1}^{2n} c_{ki} \int_\Omega \tau_j \wedge \tau_i, j = 1, 2, \ldots, 2n, \tag{10}$$

Now for any two discrete harmonic 1-forms ω and τ, assume that locally $\omega = c_1dx + c_2dy$ and $\tau = d_1dx + d_2dy$. Then

$$\omega \wedge {}^*\tau = \begin{vmatrix} c_1 & c_2 \\ -d_2 & d_1 \end{vmatrix} dx \wedge dy,$$

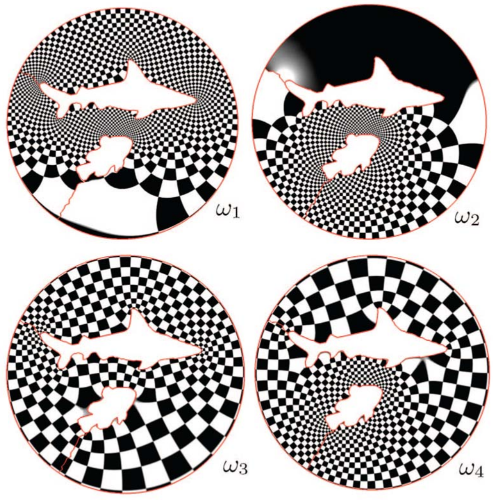

Fig. 11. Holomorphic 1-form basis.

We can treat $\omega \wedge {}^*\tau$ as a discrete 2-form, such that $\omega \wedge {}^*\tau([v_i, v_j, v_k]) = (c_1 d_1 + c_2 d_2)A_{ijk}$, where A_{ijk} is the area of $[v_i, v_j, v_k]$. Hence, the left hand side of Equation (10) can be written as

$$\begin{aligned}\int_\Omega \omega \wedge {}^*\tau &= \sum_{[v_i,v_j,v_k]\in\Sigma} \omega \wedge {}^*\tau([v_i, v_j, v_k]) \\ &= \sum_{[v_i,v_j,v_k]\in\Sigma} (\tau_1^j \tau_1^k + \tau_2^j \tau_2^k)A_{ijk}\end{aligned} \tag{11}$$

where $\tau_j = \tau_1^j dx + \tau_2^j dy$ and $\tau_k = \tau_1^k dx + \tau_2^k dy$

Equation (10) is then converted to the following linear system:

$$\sum_{[v_i,v_j,v_k]\in\Sigma} (\tau_1^j \tau_1^k + \tau_2^j \tau_2^k)A_{ijk} = \sum_{i=1}^{2n} c_{ki} \int_\Omega \tau_j \wedge \tau_i, \tag{12}$$

where $j = 1, 2, \ldots, 2n$. Similarly, the integral of the right hand side of Equation 12 can be written explicitly as:

$$\int_\Omega \tau_j \wedge \tau_i = \sum_{[v_i,v_j,v_k]\in\Sigma} (\tau_1^j \tau_2^i - \tau_2^j \tau_1^i)A_{ijk} \tag{13}$$

By solving Equation 12, we can find all the unknown coefficients and get the conjugate form. Let $\omega_k = \tau_k + i^*\tau_k$. Then $\{\omega_1, \omega_2, \ldots, \omega_{2n}\}$ forms a basis for the holomorphic 1-form group of the surface.

Fig. 11 shows the holomorphic 1-form group basis for the 2-hole planar domain.

5.2 Computational Algorithm for Shape Signature

We describe the algorithm to compute the shape signature of Ω with n inner boundary components. The inner boundaries decompose Ω into $s+1$ sub-domains Ω_k ($k = 0, 1, 2, \ldots, s$). In other words, $\Omega = \Omega_0 \cup \Omega_1 \cup \ldots \cup \Omega_s$ The algorithm consists of two main steps:

Step 1: Compute the conformal parameterizations from Ω_k onto circle domains D_k;
Step 2: Compute the conformal modules for each sub-domain Ω_k and the signature f_{ij} for each boundary.

We will now describe each step in details.

Step 1: Conformal map from Ω_k to D_k

The conformal parameterization of Ω_k can be obtained easily by computing the circular slit map and performing the Koebe's iteration. For detail, please refer to [11].

Circular slit map: The circular slit map can be obtained by finding a holomorphic 1-form ω, such that

$$\begin{aligned} Img\left(\int_{\gamma_0} \omega\right) &= 2\pi, \\ Img\left(\int_{\gamma_1} \omega\right) &= -2\pi, \\ Img\left(\int_{\gamma_k} \omega\right) &= 0,\ \ 2 \le k \le n-1. \end{aligned} \tag{14}$$

To solve Equation 14, we first express ω as a linear combination of the basis for the holomorphic 1-form group. Suppose $\omega = \sum_{k=1}^n \lambda_k \omega_k$. The coefficients $\{\lambda_k\}$ can be calculated by solving the following linear system:

$$\begin{aligned} \sum_{i=1}^n Img\left(\int_{\gamma_0} \omega_i\right)\ \lambda_i &= 2\pi, \\ \sum_{i=1}^n Img\left(\int_{\gamma_1} \omega_i\right)\ \lambda_i &= -2\pi, \\ \sum_{i=1}^n Img\left(\int_{\gamma_k} \omega_i\right)\ \lambda_i &= 0,\ \ 2 \le k \le n-1. \end{aligned} \tag{15}$$

The circular slit map is then given by:

$$\phi(p) = exp\left(\int_q^p \omega\right), \forall p \in \Omega, \tag{16}$$

where q is a base point, and the integration path is arbitrarily chosen in Ω. Fig. 6 shows the circular slit map of a 2-hole planar domain.

If Ω is a simply-connected domain (topological disk), we can compute the conformal parameterization of Ω onto the unit disk in the following way. First, we punch a small hole in the domain, and treat it as a topological annulus. Then we use the circular slit map to map the punched annulus to the canonical annulus. By shrinking the size of the punched hole, the circular slit map converges to the conformal mapping. Fig. 7 shows one such example.

Hole Filling: After computing the circular slit map, the planar domain is mapped to the planar annulus Σ with concentric circular slits. In particular, γ_0 is the unit circle, γ_1 is the inner circle and γ_k's are slits for $2 \le k \le n$. We use Delaunay triangulation to generate a disk $\mathfrak{D}_1$ bounded by γ_1 such that $\partial\mathfrak{D}_1 = \gamma_1$, and glue Σ with $\mathfrak{D}_1$ along γ_1 to obtain $\Sigma_1 := \Sigma \cup_{\gamma_1} \mathfrak{D}_1$.

We then use circular slit map again to parameterize Σ_1, such that γ_2 is opened to a circle. We compute a disk $\mathfrak{D}_2$ bounded by γ_2 and glue Σ_1 with $\mathfrak{D}_2$ to get Σ_2. By repeating the circular slit map, at step k, γ_k is opened to a circle. We compute a circular disk $\mathfrak{D}_k$ bounded by γ_k and glue Σ_{k-1} with $\mathfrak{D}_k$ to get $\Sigma_k = \Sigma_{k-1} \cup_{\gamma_k} \mathfrak{D}_k$.

Eventually, we can fill all the holes to get Σ_n.

Koebe's iterations: Note that all the disks $\mathfrak{D}_k$ in Σ_n are not exactly circular. It can be fixed by Koebe's iterations.

Through Koebe's iterations, all the boundary components become rounder and rounder. Basically, in each iteration, we choose a disk $\mathfrak{D}_k$. The complement of $\mathfrak{D}_k$ in Σ_n is a doubly-connected domain. We then map the complement to the canonical planar annulus. Hence, γ_k becomes a circle. We recompute the disk $\mathfrak{D}_k$ bounded by the updated γ_k and glue the annulus with the updated $\mathfrak{D}_k$. After this iteration, γ_k becomes a circle. Next, we choose another disk $\mathfrak{D}_j$ and repeat this process to make γ_j a circle. This will destroy the perfectness of the circular shape of γ_k. But by repeating this process, all the γ_k's become rounder and rounder, and eventually converge to perfect circles. The convergence is exponentially fast. Detailed proof can be found in [26].

Step 2: Computing $\mathbf{Mod}(D_i)$ and f_{ij}

After the conformal parameterization of Ω_k to the circle domain is computed, it has to be normalized so that a unique shape signature can be obtained. The shape signature comprises of the conformal modules and the conformal weldings f_{ij} of each boundary.

For each domains Ω_k, we denote its initial conformal parameterization by $\Phi'_k:\Omega_k \to D'_k$. First, we normalize the conformal parameterization of the outermost domain Ω_0. When the shape is embedded in the Riemann sphere S, we can normalize it by composing the initial parameterization with the Möbius transformation $\phi(z) = \frac{az+b}{cz+d}$. For example, if a shape signature is required to determine a shape up to a translation, rotation and scaling, the parameterization of the outermost domain must fix ∞. Suppose $\Phi'_k(\infty) = z_0$. Then the normalized parametrization can be obtained by composing the initial parameterization with the Möbius transformation $\phi(z) = \frac{az+b}{z-z_0}$. When the shape is embedded in the unit disk $\mathbb{D}$, the initial parametrization of the outermost domain can be normalized by the Mobiüs transformation of $\mathbb{D}$: $\phi(z) = e^{i\theta}\frac{z-a}{1-\bar{a}z}$.

After the normalized parameterization $\Phi_0:\Omega_0 \to D_0$ is computed, other initial parameterizations Φ'_k $(k = 1, 2, ...n)$ can be normalized so that: $f_{ij} = \Phi_i \circ \Phi_j^{-1}$ fixes the points $1, -1$ and i. This can be done by composing the initial parameterization with the Möbius transformation of the unit disk.

Denote the normalized conformal parameterizations by $\Phi_k:\Omega_k \to D_k$ $(k = 0, 1, 2, \ldots, n)$. We can then compute the conformal module of D_k, which can be described by its inner radii and centers. We denote it by $\mathbf{Mod}(D_k){:} = \{r_i, c_i\}_{i=1}^{n_k}$.

Now each boundary component γ_{ij} is the intersection of two adjacent domains, namely, $\gamma_{ij} = \Omega_i \cap \Omega_j$. The signature or conformal welding of γ_{ij} can be computed by $f_{ij} = \Phi_i \circ \Phi_j^{-1}$.

The conformal modules together with the conformal weldings give the shape signature of Ω:

$$S(\Omega) = \{\{r_{ij}, c_{ij}\}_{j=1}^{n_i}\}_{i=1}^{n} \cup \{f_{ij}\}_{(i,j)\in I} \tag{17}$$

The detailed algorithm for computing the shape signature of a multiply-connected shape can be summarized as in Algorithm 5.1.

Algorithm 5.1: (Computation of shape signature)

Input: Triangular meshes Ω_i $(i = 0, 1, \ldots, n)$ of each subdomains

Output: Shape signature consisting of $\mathbf{Mod}(D_i){:} = \{r_{ij}, c_{ij}\}_{j=1}^{n_i}$ and $\{f_{ij}\}_{(i,j)\in I}$ for $i = 0, 1, \ldots, n$

1) For each i, compute the holomorphic 1-form ω_i to obtain the circular slit map of Ω_i
2) Apply the hole-filling algorithm on the circular slit map and Koebe's iteration to obtain the conformal parameterization of Ω_i
3) Normalize the conformal parameterizations to obtain a normalized conformal modules $\mathbf{Mod}(D_i){:} = \{r_{ij}, c_{ij}\}_{j=1}^{n_i}$
4) Obtain the conformal welding $\{f_{ij}\}_{(i,j)\in I}$ using Equation (7)

5.3 Reconstruction of Shapes from their Signatures

Every planar multiply-connected domain Ω is associated with a unique shape signature $S(\Omega)$. As described in Section 3, given the shape signature $S(\Omega)$, its associated shape Ω can be reconstructed, which is unique up to a Möbius transformation. The conformal ambiguity can be further removed by suitable normalization.

In Section 3, we describe that, in the continuous case, a shape can be reconstructed from its shape signature by solving the Beltrami equation. More specifically, given a shape signature $S(\Omega)$, we can obtain a Beltrami coefficient μ_Γ corresponding to $S(\Omega)$. The associated shape can then be reconstructed by computing the quasi-conformal map G_Γ with the Beltrami coefficient μ_Γ. In particular, the associated shape Ω is given by $\Omega = G_\Gamma(S_0) \cup G_\Gamma(S_1) \cup ... \cup G_\Gamma(S_n)$ (See Fig. 9). In the discrete case, the computation of the quasi-conformal map can be more direct without explicitly solving the Beltrami equation. Given a triangular mesh of the Riemann sphere S (or unit disk $\mathbb{D}$), the angle structure of the mesh can be deformed according to the Beltrami coefficient. As a result, the computation of the quasi-conformal map will be converted to the computation of the conformal map under the deformed angle structure.

More specifically, from the Beltrami coefficient μ_Γ, one can deform the conformal structure of S_k to that of Ω_k. Under the conformal structures of Ω_k, $G_\Gamma:S \to \Omega$ becomes a conformal mapping. The conformal structure of Ω_k is equivalent to that of D_k, therefore, one can use the conformal structure of D_k directly. In the discrete case, the conformal structure is represented by the angle structure (5.1). Therefore in our algorithm, we copy the angle structures of D_k's to S, and compute the conformal map under the deformed angle structure directly. For details, we refer the readers to [14].

In summary, the reconstruction algorithm can be divided into two main steps:

Step 1: Glue the circle domains together;
Step 2: Compute the conformal map under the deformed angle structure for shape reconstruction.

Below we describe each steps in details.

Step 1: Glueing of the circle domains

Given a shape signature $S(\Omega) = \{\mathbf{Mod}(D_k)\}_{k=0}^{n} \cup \{f_{ij}\}_{(i,j)\in I}$. We first construct the circle domains D_k's directly from their conformal modules $\mathbf{Mod}(D_k)$'s. This can done by tessellating the circular boundaries of each D_k and triangulating D_k using Delaunay triangulation. The triangular meshes D_i and D_j are then combinatorially glued together by the conformal welding f_{ij}. Suppose the boundary circle $\gamma_i \in \partial D_i$ corresponds to $\gamma_j \in \partial D_j$, hence $f_{ij}:\gamma_i \to \gamma_j$. For each vertex $v_i \in \gamma_i$, we insert $f_{ij}(v_i)$ to γ_j. And vice versa, for each vertex $v_j \in \gamma_j$, we insert $f_{ij}^{-1}(v_j)$ to γ_i. With the newly inserted vertices on ∂D_i and ∂D_j, we use constrained Delaunay triangulation to refine the triangulation of D_i and D_j. The refined triangular mesh D_i and D_j can therefore be combinatorially glued through γ_i and γ_j, by identifying $v_k \in \partial D_i$ with $f_{ij}(v_k) \in \partial D_j$. This process is repeated for all f_{ij}'s, to obtain a combinatorial simply-connected triangular mesh. We denote it by D (which is a triangular mesh of either the Riemann sphere or the unit disk).

Step 2: Shape reconstruction

Now, the angle structure $A(d)$ of the combinatorial triangular mesh D can be computed. In fact, $A(d) = \cup_{k=0}^{n} A(D_k)$. The mesh D with respect to the angle structure $A(d)$ can then be conformally parameterized onto a triangular mesh of the unit disk (or Riemann sphere if the shape is embedded in the whole plane). We compute the conformal parameterization G_Γ as described in Section 5.2. The original shape Ω can then be reconstructed by $\Omega = G_\Gamma(S_0) \cup G_\Gamma(S_1) \cup \ldots \cup G_\Gamma(S_n)$.

The detailed shape reconstruction algorithm can now be summarized as in Algorithm 5.2

Algorithm 5.2: (Shape reconstruction)

Input: Shape signature consisting of $\mathbf{Mod}(\mathbf{D_i}) := \{r_{ij}, c_{ij}\}_{j=1}^{n_i}$ $(i = 0, 1, \ldots, n)$ and $\{f_{ij}\}_{(i,j)\in I}$

Output: Shape Ω corresponding to the shape signature

1) *Construct the circle domains D_i's directly from the conformal modules $\mathbf{Mod}(D_i)$'s*
2) *Use constrained Delaunay triangulation to refine the triangulation of D_i's based on the conformal welding $\{f_{ij}\}_{(i,j)\in I}$*
3) *Combinatorially glue the refined triangular meshes of D_i's to obtain a combinatorial simply-connected triangular mesh D*
4) *Equip D with the angle structure $A(d) = \cup_{k=0}^{n} A(D_k)$, and compute the conformal parameterization G_Γ of D*
5) *Reconstruct the shape Ω by $\Omega = G_\Gamma(S_0) \cup G_\Gamma(S_1) \cup \ldots \cup G_\Gamma(S_n)$.*

6 Experimental Results

Implementation: Our proposed algorithm is implemented on a generic C++ windows XP platform, with Intel Duo CPU 2.33 GHz, 3.98G RAM. The numerical systems are solved using Matlab C++ library. The contour extraction is obtained using the OpenCV library. The computational time for our algorithm is shown in Tables 1 and 2. In general, both the signature calculation and reconstruction process take less than 1 minute to compute, even on complicated domains.

Shape signature: In Fig. 12, we demonstrate the process of computing the shape signature $S(\Omega)$ of a double fish image. Given the original image, we first perform image segmentation to get the binary image. We then calculate the contours of the objects in the image. The contour of each fish is shown in the figure. For simplicity, we treat the outermost boundary of the image as the unit circle. Then all the contours segment the image into three sub-domains, namely, $\Omega_0, \Omega_1, \Omega_2$. We conformally map each connected sub-domain to a circle domain as shown in (a). Ω_0 is mapped to a disk D_0 with two circular holes. The centers and radii (c_0, r_0) and (c_1, r_1) represent the conformal module of Ω_0. Ω_1 and Ω_2 are mapped to the unit disks D_1 and D_2 respectively. We denote the conformal maps of Ω_i by $\Phi_i:\Omega_i \to D_i$ $(i = 0, 1, 2)$. The contour of the small fish are mapped to the boundary of D_1 and one inner boundary of D_0. Its conformal welding is given by $f_{01} := \Phi_1 \circ \Phi_0^{-1}$, which is shown in (b) as the blue curve. Here, the diffeomorphisms from circle to circle is considered as a monotonic function from $[0, 2\pi]$ to itself. Similarly, the conformal welding f_{02} of the contour of the shark can also be computed, which is also shown in (b) as the red curve. The shape signature of the double fish image is given by $S(\Omega) = \{c_0, c_1, r_0, r_1, f_{01}, f_{02}\}$.

Fig. 13(a) shows another double fishes image with spatial changes in the positions of the two fishes. Compared with Fig. 12, the big shark and small fish interchanged their positions. The shape signature of the image is shown in Fig. 13(b), which is quite different from the shape signature in Fig. 12 (see red and blue curves). In other words, our shape signature can effectively capture spatial changes of objects in the image.

TABLE 1
Computational Time (Second) for Signature

Model	#(contour)	#(face)	Signature
Cat	3	10236	19 s
TwoCats	6	11680	29 s
Ameba	2	17930	8 s
Fishes	2	11716	23 s
NewFishes	2	14780	24 s
Elephant	2	23678	17 s
Brain	2	16164	11 s
Wolf	3	16644	47 s
Flower	2	13944	10s
Mickey	3	14854	16s
BigEyeFish	2	13072	9s

TABLE 2
Computational Time (Second) for Reconstruction

Model	#(contour)	#(face)	Reconstruction
Cat	3	10236	10s
TwoCats	6	11680	7s
Ameba	2	17930	12s
Fishes	2	11716	8s

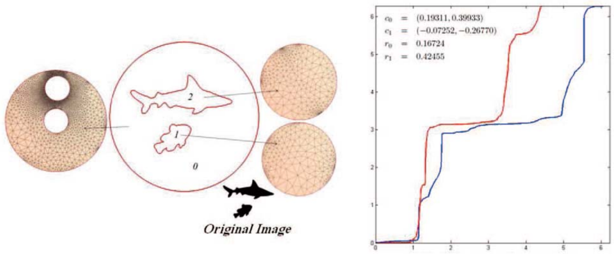

(a) (b)

Fig. 12. (a) Each segment is mapped to a circle domains. (b) Conformal modules (centers and radii of inner circles) of the circle domains and conformal weldings define the shape signature.

Fig. 14 shows the shape signatures of five different images with 2 boundaries and 2 levels (levels = number of multiply-connected sub-domains). The first row shows the shape signature of the flower image. Note that the fluctuating pattern of the outer boundary of the flower is effectively captured by f_{01} (the red curve). The other rows show the shape signatures of the fish, brain, elephant and ameba images respectively. The five different images have very different shape signatures.

We also apply this algorithm to detect shape differences between brain shapes extracted from MR images. Each brain shape has 2 boundaries and 2 levels. Fig. 15 shows three brain shapes and their associated shape signatures. The original MR images and their associated contours are shown on the left column. Their corresponding shape signatures are shown on the right column. Note that the patterns of the conformal weldings of each shapes look similar. But the details of the shape signatures are obviously different. Our proposed signature can potentially be used for medical shape analysis.

Fig. 16 shows the shape signatures of two different images with 3 boundaries and 2 levels. The top shows the contours of the Mickey mouse image, which consists of 3 contours. The exterior and interior of the domain are conformally parameterized. The conformal domains consist of two circle domains, and their conformal modules consist of 3 centers and 3 radii. The conformal modules together with the conformal weldings define the shape signature, which is shown on the right column. The bottom shows the shape signature of a cat image also with 3 boundaries and 2 levels. The corresponding shape signature is as shown in the right column, which is very different from the shape signature of the Mickey mouse image.

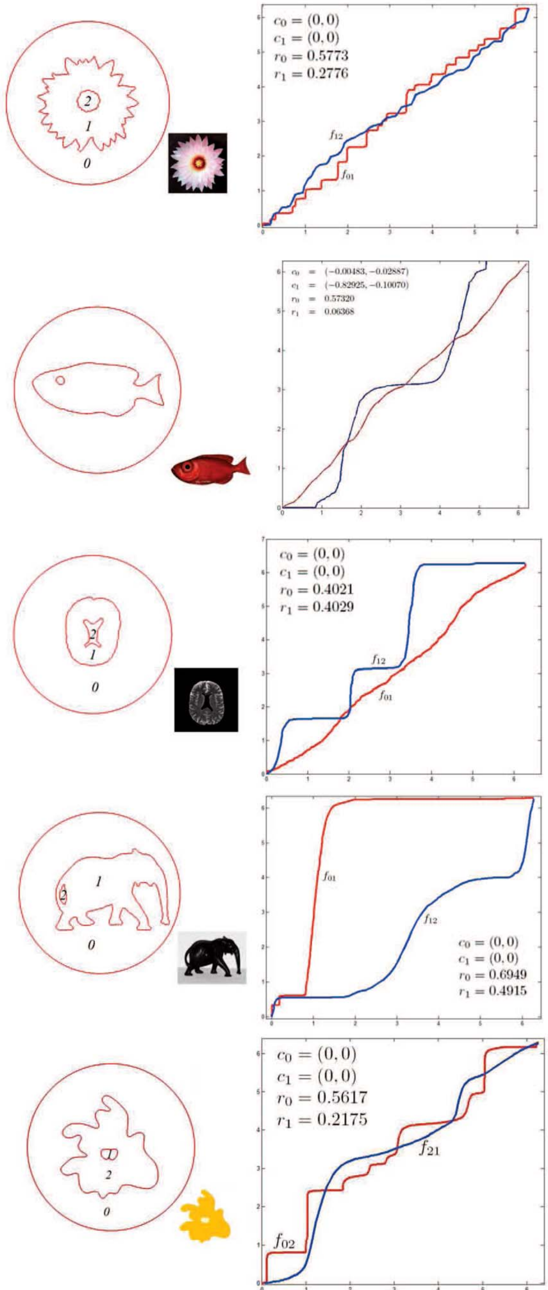

Fig. 14. Shape signatures of different images with 2 boundaries and 2 levels. The original images and their associated contours are shown in the left column. Their corresponding shape signatures are shown in the right column.

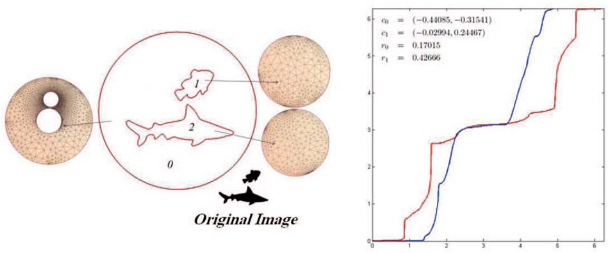

(a) (b)

Fig. 13. (a) Shark image with spatial changes in the positions of the two fishes. (b) Shape signature. The shape signature can effectively capture spatial changes of objects in the image (compared to Fig. 12).

Fig. 17 shows a wolf image with 3 boundaries and 1 level. The exterior and interior of the domain are conformally mapped to circle domains. The conformal domains consist of one circle domain with 3 inner disks removed, as shown on the left. Hence, the conformal modules consist of 3 centers and 3 radii. The shape signature of the image is as shown in the right column.

We also computed the shape signatures on more complicated images. Fig. 18 shows an image with two cats. It consists of 6 boundaries with 2 levels. The conformal domains comprise of 3 circle domains with 3 holes

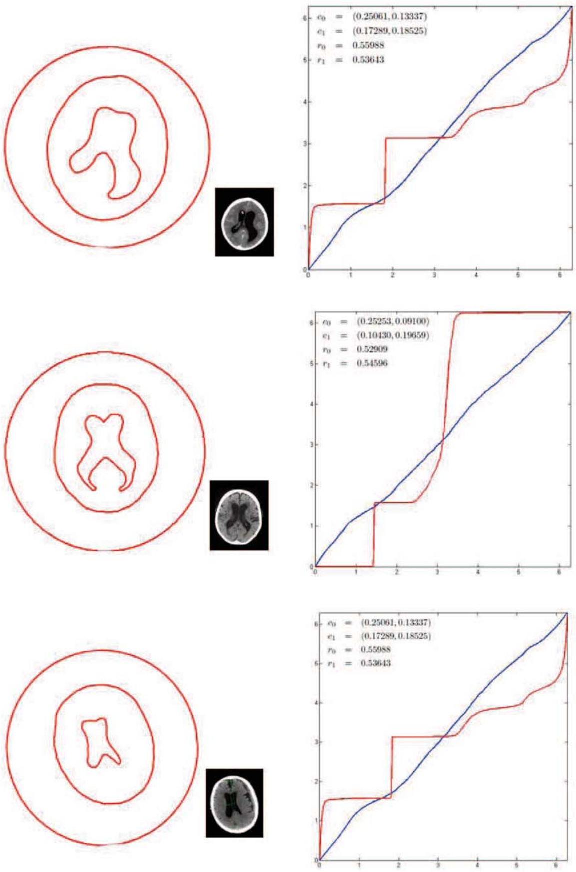

Fig. 15. Shape signatures of three brain shapes extracted from MR images. Each shape has 2 boundaries and 2 levels. The original images and their associated contours are shown in the left column. Their corresponding shape signatures are shown in the right column.

removed. Hence, the conformal modules consist of 6 centers and 6 radii. The shape signatures are plotted on the right column. The top shows the signature for the outer level whereas The bottom shows the signature of the inner level.

Shape clustering: In Section 4, we propose a shape distance defined on the space of all shape signatures.The shape distance provides us a useful tool to quantitatively measure the geometric differences between different multiply-connected objects. In order to demonstrate the effectiveness of the shape distance to measure geometric differences, a shape clustering experiment for a collection of shapes have been carried out. In Fig. 21, we show a collection of multiply-connected shapes from three different categories, namely, 1. fish; 2. brain and 3. tool. They are randomly distributed and our goal is to cluster them into their corresponding categories using our proposed shape signature and shape distance. Using the k-mean method, we cluster the randomly distributed collection of multiply-connected shapes into three categories. The clustering result is shown in Fig. 22. As shown in the figure, the shapes can be successfully clustered into their corresponding groups. Fig. 23 shows the signatures of the collection of shapes. (a) shows the signature corresponding to the outer boundary. (b) shows the signature corresponding to the inner boundary. They are colored according to the clustering result.

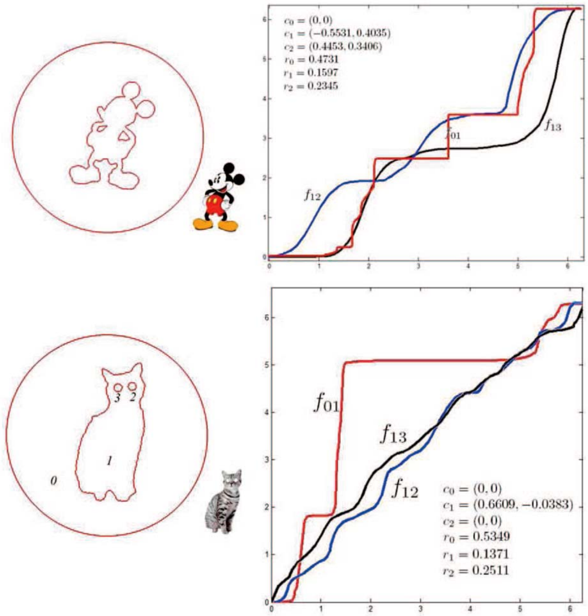

Fig. 16. Shape signatures of different images with 3 boundaries and 2 levels.

Observe that the signatures of shapes in the same category are similar. It demonstrates that our proposed shape signature can be an effective candidate for shape clustering.

Shape signature with added noises: We have examined the sensitivity of our proposed shape signature to noises. We synthetically add noises to the contours of a shape and compute its associated shape signature. In Fig. 19, noises are added to the outer boundary of the ameba, brain and elephant shapes respectively. The inner contours of the shapes remains unchanged. Their associated shape signatures are computed and are shown in the right column. Note that their shape signatures are very similar to the shape signatures of their original shapes (compared to the shape signatures as shown in Fig. 14). The signatures of the inner contours are almost the same. The shape distances between the original shape signatures and the noisy shape signatures are also computed, as shown in Table 3. The shape distances are all less than 0.09, which is very small. It shows that our proposed shape signature is stable under noises.

Shape reconstruction: Fig. 20 shows the reconstruction of the double fish image from its shape signature. The reconstructed shape closely resembles to the original shape, except some very tiny details are smoothed out (as shown

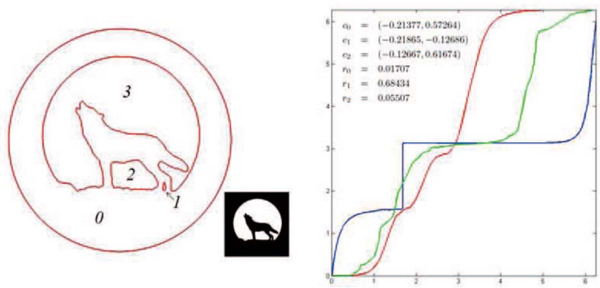

Fig. 17. Shape signatures of the wolf image with 3 boundaries and 1 levels.

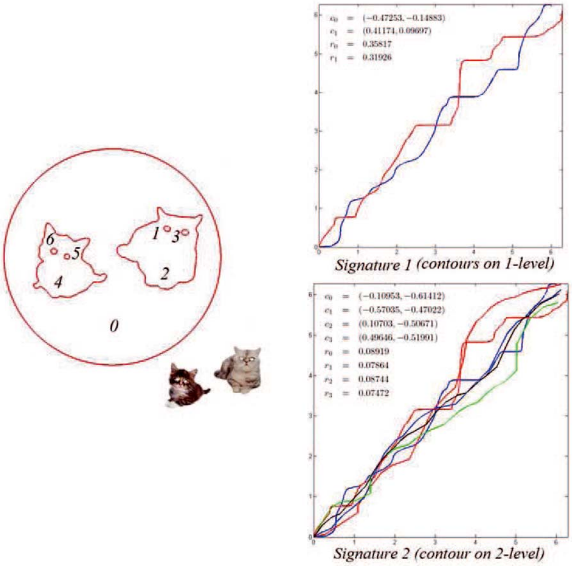

Fig. 18. Shape signature of the double cat image with 6 boundaries and 2 levels.

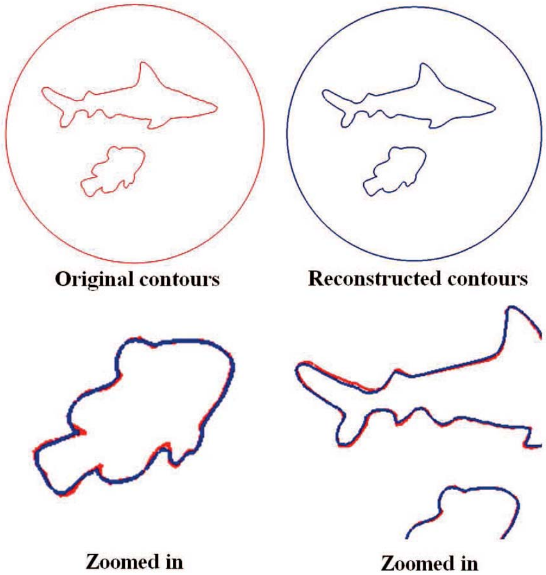

Fig. 20. Top row shows the comparison between the original contours and the reconstructed ones. The bottom row shows the zoomed views. It shows that the reconstructed ones are smoother.

in the zoomed views). It shows our algorithm can effectively reconstruct shapes from their signatures. We also tested our reconstruction algorithm on images with 2 levels. Fig. 24(top) shows the Ameba image with 2 boundaries and 2 levels. We reconstruct the image from its shape signature, which is very close to the original image. Fig. 24(bottom) shows a cat image with 3 boundaries and 2 levels. The original contour of the cat image is a bit noisy. We compute the shape signature of the image and reconstruct the contours from the computed shape signature. The reconstructed image is shown on the right. Again, the reconstructed image is very close to the original one, although some tiny details of the original noisy contours are smoothed out a little bit.

Finally, we studied the numerical error of our reconstruction scheme. Table 4 shows the distance between the original and reconstructed contours of the Ameba and cat

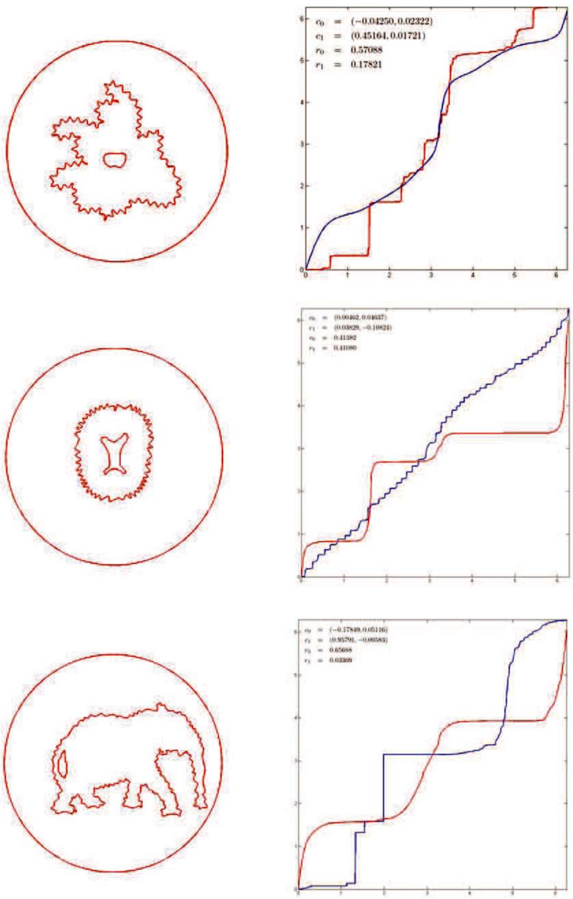

Fig. 19. Shape signatures of the ameba, brain and elephant shapes with noise added to the outer boundaries.

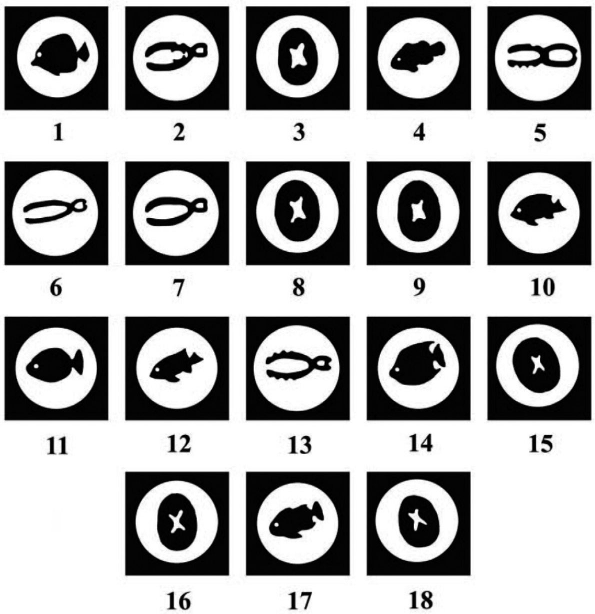

Fig. 21. Collection of shapes from three different categories (fish, brain and tool), which are randomly distributed. Our goal is to cluster them using our proposed shape distance.

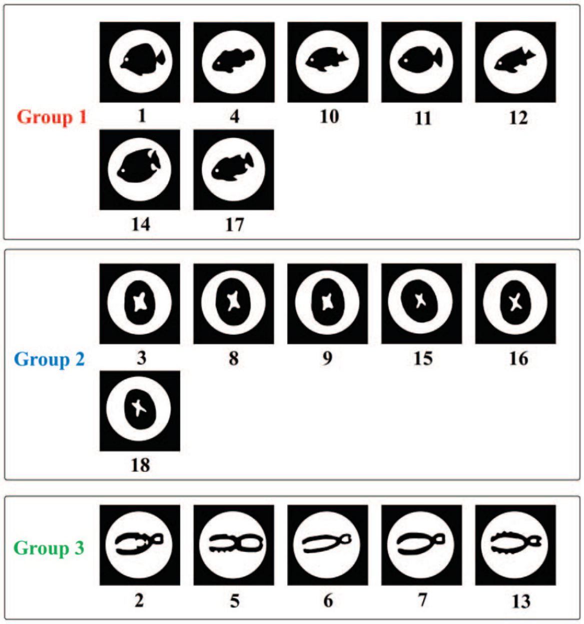

Fig. 22. Shape clustering result of the collection of shape given in Fig. 21, using our proposed shape distance.

images. It shows a very small numerical error. The average distance is less than 0.005. It means our proposed reconstruction algorithm is accurate.

Shape morphing: Our algorithm can also be applied to shape morphing. Shape morphing refers to the process of interpolation between two different shapes, which plays an important role in animation. Our shape signature and reconstruction scheme allows us to easily perform a morphing between two multiply-connected object.

Given two different multiply-connected shapes Ω_1 and Ω_2. We compute their associated shape signatures. Each

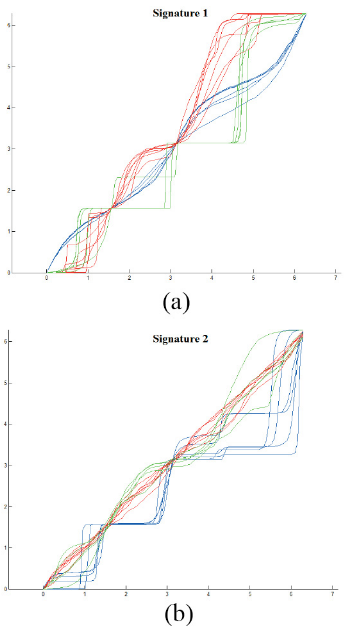

Fig. 23. Signatures of the collection of shapes given in Fig. 21, colored according to the clustering result. (a) Shows the signature corresponding to the outer boundary. (b) Shows the signature corresponding to the inner boundary.

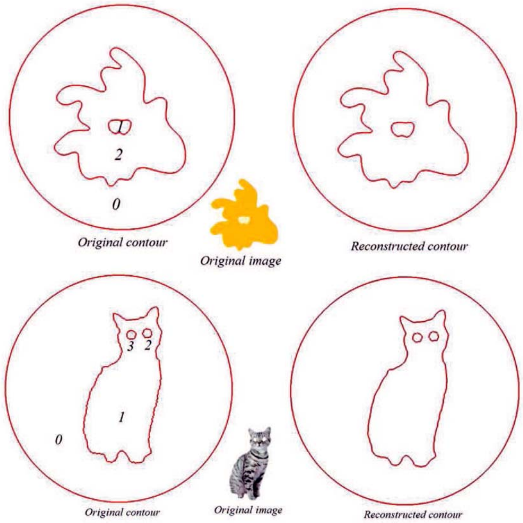

Fig. 24. Reconstruction of the ameba image and the cat image from their shape signatures.

shape signature Υ_i $(i = 1, 2)$ is associated with a quasi-conformal map G_{Υ_i}, which can be used to reconstruct the multiply-connected shape Ω_i (see Section 3). Each quasi-conformal map G_{Υ_i} is associated with a Beltrami coefficient μ_i. An interpolation between μ_1 and μ_2 can be performed. Mathematically, we can find $\mu(t)$ for $0 \leq t \leq 1$ such that $\mu(0) = \mu_1$ and $\mu(1) = \mu_2$. We can then reconstruct the corresponding quasi-conformal map $G(t)$ associated with $\mu(t)$ for $0 \leq t \leq 1$. Hence, the intermediate shape $\Omega(t)$ corresponding to $\mu(t)$ can be constructed, with $\Omega(0) = \Omega_1$ and $\Omega(1) = \Omega_2$. $\Omega(t)$ gives a morphing between the two multiply-connected shapes Ω_1 and Ω_2. Note that in classical Teichmüller theory, each point in the Teichmüller space represents a Riemann surface (in our case, Riemann surfaces are multiply-connected domains). The path given by the interpolation between the Beltrami coefficient represents a geodesic between the two Riemann surfaces under the Teichmüller metric.

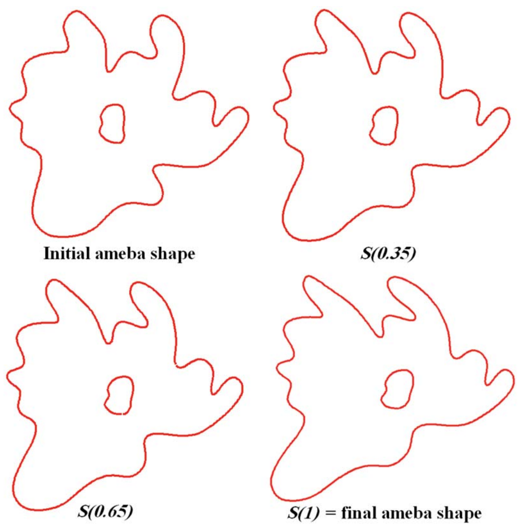

Fig. 25. Morphing between two ameba images.

TABLE 3
Shape Distance between the Original and Noisy Shapes

Shape 1	Shape 2	Distance
Ameba	Noisy ameba	0.0050
Brain	Noisy brain	0.0846
Elephant	Noisy elephant	0.0711

Fig. 25 shows the morphing result between an initial ameba shape and a final ameba shape. The shape signatures of the initial ameba shape and the final ameba shape are computed. We denote them by $S_{initial}$ and S_{final} respectively. Then we find an interpolation $S(t)$ between $S_{initial}$ and S_{final}, such that $S(0) = S_{initial}$ and $S(1) = S_{final}$. The intermediate shape associated with the shape signature $S(t)$ can then be reconstructed. Fig. 25 shows the intermediate shapes between the initial and final ameba shapes. Experimental result shows that the morphing is smooth. In Fig. 26, we show the morphing result between an initial brain shape and a final brain shape. The intermediate shapes between the initial and final brain shapes are shown. Again, it demonstrates a smooth morphing between the two brain shapes.

7 Conclusion

In this paper, we propose a novel shape signature to represent 2D multiply-connected objects using conformal weldings and conformal modules. A metric can be defined on the proposed representation space, which measures dissimilarities between objects of general topologies. The basic idea is to conformally map the interior and exterior domains to unit disks and circle domains using holomorphic 1-forms. A set of diffeomorphisms of the unit circle (called the conformal weldings) can be obtained, which together with the conformal modules can be used to define the shape signature. The shape signature uniquely determines its associated shape under a suitable normalization. Hence, the shape signature can be considered as a fingerprint of the multiply-connected object. In this paper,

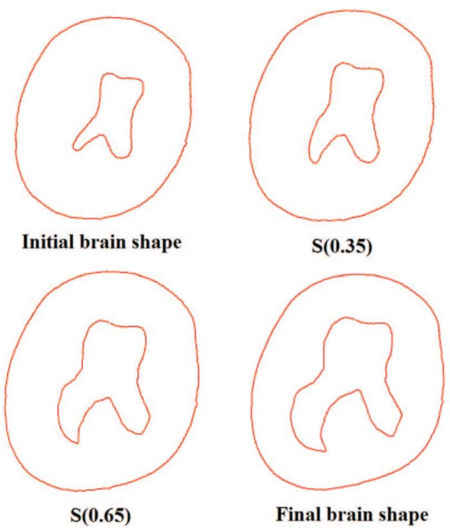

Fig. 26. Morphing between two brain shapes.

TABLE 4
Distance between the Original and Reconstructed Contours

Ameba	# of vertex	Distance sum	Average distance
Contour 1	685	1.669626	0.002437
Contour 2	112	0.238269	0.002127
Cat	**# of vertex**	**Distance sum**	**Average distance**
Contour 1	96	0.227687	0.002372
Contour 2	92	0.295533	0.003212
Contour 3	363	1.674350	0.004613

we introduce a reconstruction algorithm to obtain shapes from their shape signatures by solving the Beltrami equation. This completes the framework and allows us to move back and forth between shapes and their signatures. A morphing algorithm can also be developed by interpolating the Beltrami coefficients associated with the shape signatures of different shapes. We test the proposed framework on real images to compute their shape signatures. Experimental results of the shape clustering for a collection of multiply-connected objects demonstrate the effectiveness of the proposed shape signature to distinguish shapes.

Nevertheless, the current proposed model still has some limitations. Firstly, the current computation for the Koebe's iterations requires dense triangulation, which has high storage requirement. We are therefore seeking for a mesh free method to reduce storage requirement and further improve the efficiency. Secondly, the current model is vulnerable to topological noises. If the segmentation result is not good, extra holes (or islands) will be created. The obtained signature will then be completely different. We are looking for measures to cope with this limitation.

Finally, we believe the proposed shape signature will open up several other interesting research directions. One interesting direction is to explore different metrics on the proposed signature space. There are several metric for the Teichmüller space from the quasi-conformal Teichmüller theory. We will examine which metric is the best for the purpose of shape analysis and develop efficient algorithms to compute the metric. Another direction is to generalize the proposed algorithm to analyze surface curves defined on Riemann surfaces with arbitrary topologies. It will be useful for the shape analysis of features on anatomical structures in medical morphometry. Last but not least, experimental results suggest that our method can effectively combine with other statistical shape analysis methods and machine learning methods for shape clustering and shape analysis. We will explore this research direction in more details and apply it to medical shape analysis problems.

Acknowledgments

L. Ming Lui is supported by RGC GRF (Project ID: 401811)and CUHK Direct Grant (Project ID: 2060413). Xianfeng Gu is supported in part of NSF Nets 1016286, NSF IIS 0916286, NSF CCF 1081424 and ONR N000140910228.

References

[1] S. C. Zhu and A. L. Yuille, "A flexible object recognition and modeling system," *Int. J. Comput. Visions*, vol. 20, no. 3, pp. 187–212, 1996.

[2] T. Liu and D. Geiger, "Approximate tree matching and shape similarity," in *Proc. 7th IEEE Int. Conf. Computer Vision*, Kerkyra, Greece, 1999, pp. 456–462.
[3] S. Belongie, J. Malik, and J. Puzicha, "Shape matching and object recognition using shape contexts," *IEEE Trans. Pattern Anal. Mach. Intell.*, vol. 24, no. 4, pp. 509–522, Apr. 2002.
[4] F. Mokhtarian and A. Mackworth, "A theory of multiscale, curvature-based shape representation for planar curves," *IEEE Trans. Pattern Anal. Mach. Intell.*, vol. 14, no. 8, pp. 789–805, Aug. 1992.
[5] A. Ericsson and K. Astrom, "An affine invariant deformable shape representation for general curves," in *Proc. IEEE Int. Conf. Computer Vision*, Nice, France, 2003, pp. 1142–1149.
[6] T. Sebastian, P. Klein, and B. Kimia, "Shock based indexing into large shape databases," in *Proc. 7th European Conf. Computer Vision*, Copenhagen, Denmark, 2002, pp. 731–746.
[7] I. Dryden and K. Mardia, *Statistical Shape Analysis*. New York, NY, USA: Wiley, 1998.
[8] Q. Yang and S. Ma, "Matching using schwarz integrals," *Pattern Recognit.*, vol. 32, no. 6, pp. 1039–1047, Jun. 1999.
[9] S. M. Lee, N. A. Clark, and P. A. Araman, "A shape representation for planar curves by shape signature harmonic embedding," in *Proc. IEEE Computer Soc. Conf. CVPR*, Vol. 2. Washington, DC, USA, 2006, pp. 1940–1947.
[10] Y. Lipman and T. Funkhouser, "Möbius voting for surface correspondence," *ACM Trans. Graphics*, vol. 28, no. 3, Article 72, 2009.
[11] W. Zeng, Y. Zeng, Y. Wang, X. Yin, X. Gu, and D. Samaras, "3D non-rigid surface matching and registration based on holomorphic differentials," in *Proc. 10th ECCV*, Marseille, France, pp. 1–14, 2008.
[12] W. Zeng, L. M. Lui, X. Gu, and S. T. Yau, "Shape analysis by conformal modules," *Methods Appl. Anal.*, vol. 15, no. 4, pp. 539–556, 2008.
[13] W. Zeng, S. Samaras, and X. Gu, "Ricci flow for 3D shape analysis," *IEEE Trans. Pattern Anal. Mach. Intell.*, vol. 32, no. 4, pp. 662–677, Apr. 2010.
[14] W. Zeng, L. M. Lui, F. Luo, T. F. Chan, S. T. Yau, and X. Gu, "Computing quasiconformal maps using an auxiliary metric and discrete curvature flow," *J. Numer. Math.*, vol. 121, no. 4, pp. 671–703, 2012.
[15] E. Sharon and D. Mumford, "2D-shape analysis using conformal mapping," *Int. J. Comput. Vision*, vol. 70, no. 1, pp. 55–75, 2006.
[16] E. Hildreth, *The Measurement of Visual Motion*, Cambridge, MA, USA: MIT Press, 1984.
[17] M. Kass, A. Witkin, and D. Terzopoulos, "Snakes: Active contour models," *Int. J. Comput. Vision*, vol. 1, no. 4, pp. 321–331, 1988.
[18] S. Ullman, "Aligning pictorial descriptions: An approach to object recognition," *Cognition*, vol. 32, no. 3, pp. 193–254, 1989.
[19] Y. Amit, U. Grenander, and M. Piccioni, "Structural image restoration through deformable templates," *J. Amer. Statist. Assoc.*, vol. 86, no. 414, pp. 376–387, 1991.
[20] A. Yuille, "Deformable templates for face recognition," *J. Cognit. Neurosci.*, vol. 3, no. 1, pp. 59–71, 1991.
[21] F. P. Gardiner and N. Lakic, *Quasiconformal Teichmüler Theory*. Providence, RI, USA: American Mathematical Society, 1999.
[22] K. Astala, T. Iwanieg, and G. Martin, *Elliptic Partial Differential Equations and Quasiconformal Mappings in the Plane*. Princeton, NJ, USA: Princeton University Press, 2009.
[23] P. Henrici, *Applied and Computational Complex Analysis*. New York, NY, USA: Wiley Classics Library, 1974.
[24] W. Zeng, X. T. Yin, M. Zhang, F. Luo, and X. Gu, "Generalized Koebe's method for conformal mapping multiply connected domains," in *Proc. SIAM/ACM Joint Conf. Geometric Physical Modeling*, New York, NY, USA, 2009, pp. 89–100.
[25] L. M. Lui, W. Zeng, X. Gu, T. F. Chan, and S. T. Yau, "Shape analysis of planar objects with arbitrary topologies using conformal geometry," in *Proc. 11th European Conf. Computer Vision*, Heraklion, Greece, 2010, pp. 672–686.
[26] P. Henrici, *Applied and Computational Complex Analysis, Discrete Fourier Analysis, Cauchy Integrals, Construction of Conformal Maps, Univalent Functions*, vol. 3. New York, NY, USA: Wiley-Interscience, 1993.
[27] L. V. Ahlfors, *Complex Analysis*. New York, NY, USA: McGraw-Hill, 1953.
[28] A. Trouvé, "Diffeomorphisms groups and pattern matching in image analysis," *Int. J. Comput. Visions*, vol. 28, no. 3, pp. 213–221, Jul. 1998.
[29] P. Dupuis, U. Grenander, and M. Miller, "Variational problems on flows of diffeomorphisms for image matching," *Quart. Appl. Math.*, vol. 56, no. 3, p. 587, 1998.
[30] M. Miller, A. Trouvé, and L. Younes, "On the metrics and Euler-Lagrange equations of computational anatomy," *Annu. Rev. Biomed. Eng.*, vol. 4, pp. 375–405, Aug. 2002.
[31] A. Trouvé and L. Younes, "Local geometry of deformable templates," *SIAM J. Math. Anal.*, vol. 37, no. 1, pp. 17–59, Aug. 2006.
[32] M. Miller, A. Trouvé, and L. Younes, "Geodesic shooting for computational anatomy," *J. Math. Imaging Visions*, vol. 24, no. 2, pp. 209–228, 2006.
[33] L. Younes, "Spaces and manifolds of shapes in computer vision: An overview," *Image Vision Comput.*, vol. 30, no. 6–7, pp. 389–397, 2012.
[34] P. Michor and D. Mumford, "Riemannian geometries on spaces of plane curves," *J. Eur. Math. Soc.*, vol. 8, no. 1, pp. 1–48, 2006.
[35] P. Michor and D. Mumford, "Riemannian geometries on spaces of plane curves," *Appl. Comput. Harmonon. Anal.*, vol. 23, no. 1, pp. 74–113, 2007.
[36] L. Younes, *Shapes and Diffeomorphisms*. Heidelberg, Germany: Springer, 2010.
[37] M. Meyer, M. Desbrun, P. Schröder, and A. H. Barr, "Discrete differential-geometry operators for triangulated 2-manifolds," in *Visualization and Mathematics III*. Berlin, Germany: Springer, 2003, pp. 35–57.

Lok Ming Lui received the Ph.D. degree in applied mathematics from the University of California at Los Angles, Los Angeles, CA, USA, in 2008. He is an Assistant Professor with the Department of Mathematics, Chinese University of Hong Kong (CUHK), Hong Kong. Before joining CUHK, he was a Post-Doctoral Scholar for 2 years with the Department of Mathematics, Harvard University, Cambridge, MA, USA. His current research interests include computational conformal and quasi-conformal geometry, Teichmuller theory, surface registration, medical imaging, and shape analysis.

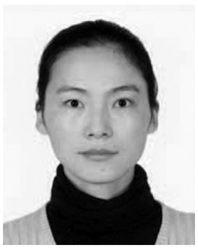

Wei Zeng received the Ph.D. degree from the Institute of Computing Technology, Chinese Academy of Sciences, Microsoft Research Asia, in 2008. She is an Assistant Professor with the School of Computing and Information Sciences, Florida International University, Miami, FL, USA. She was a Research Scholar with the Department of Computer Science at Stony Brook University, Stony Brook, NY, USA, in 2006 to 2009. Her current research interests include computational conformal geometry and shape analysis, including surface parameterization, surface matching, registration, tracking, and recognition.

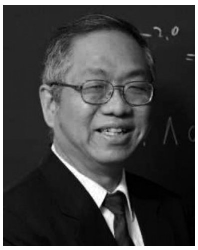

Shing-Tung Yau received the Ph.D. degree in mathematics from the University of California at Berkeley, CA, USA, in 1971. He is Professor with the Department of Mathematics, Harvard University, Cambridge, MA, USA. His work is mainly in differential geometry, especially in geometric analysis. His contributions have had an influence on both physics and mathematics and he has been active at the interface between geometry and theoretical physics. Recently, he has been interested in using differential geometry in engineering applications. In particular, his works focus on applying conformal geometry for face recognition, shape analysis, computer graphics, computer vision, and medical imaging.

Xianfeng Gu received the Ph.D. degree in computer science from Harvard University, Cambridge, MA, USA, in 2003. He is an Associated Professor of Computer Science and the Director of the 3D Scanning Laboratory with the Department of Computer Science at Stony Brook University, Stony Brook, NY, USA. His current research interests include computer vision, graphics, geometric modeling, and medical imaging. His major works include global conformal surface parameterization in graphics, tracking and analysis of facial expression in vision, manifold splines in modeling, brain mapping and virtual colonoscopy in medical imaging, and computational conformal geometry. He won the U.S. National Science Foundation CAREER Award in 2004.